iScience

CellPress
OPEN ACCESS

Article

# PTEN acts as a crucial inflammatory checkpoint controlling TLR9/IL-6 axis in B cells

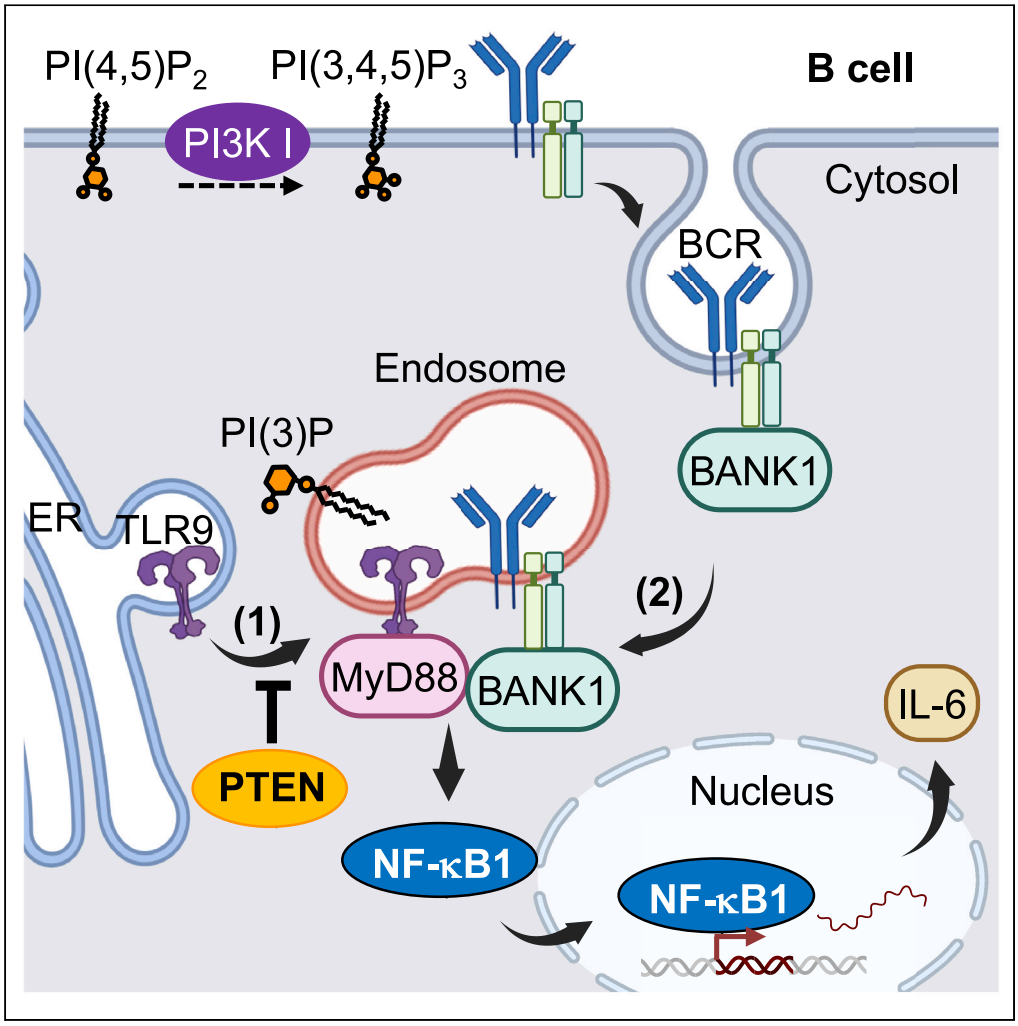


Pei-Ju Tsai, Ming-Yu Chen, Wei-Chan Hsu, ..., Tsung-Hsien Chuang, Guann-Yi Yu, Yu-Wen Su

yuwensu@nhri.edu.tw

## Highlights

Mature B cell-specific PTEN-deleted mice develop spontaneous inflammation

PTEN deficiency in B cells leads to increased TLR9 endosomal localization (Signal 1)

The increased IL-6 production mediated by TLR9 requires a functional BCR (Signal 2)

Ectopic BCR expression on non-inflammatory PTEN-deficient B cells induces inflammation

Tsai et al., iScience *27*, 110388
July 19, 2024 
https://doi.org/10.1016/j.isci.2024.110388

iScience

CellPress
OPEN ACCESS

Article

# PTEN acts as a crucial inflammatory checkpoint controlling TLR9/IL-6 axis in B cells

Pei-Ju Tsai,[1] Ming-Yu Chen,[1] Wei-Chan Hsu,[1] Su-Fang Lin,[2] Po-Chiang Chan,[1] Hsin-Hsin Chen,[1] Cheng-Yuan Kao,[1] Wen-Jye Lin,[1] Tsung-Hsien Chuang,[1] Guann-Yi Yu,[3] and Yu-Wen Su[1,4,*]

## SUMMARY

**Phosphatase and tensin homolog (PTEN) is vital for B cell development, acting as a key negative regulator in the PI3K signaling pathway. We used CD23-cre to generate PTEN-conditional knockout mice (CD23-cKO) to examine the impact of PTEN mutation on peripheral B cells. Unlike mb1-cre-mediated PTEN deletion in early B cells, CD23-cKO mutants exhibited systemic inflammation with increased IL-6 production in mature B cells upon CpG stimulation. Inflammatory B cells in CD23-cKO mice showed elevated phosphatidylinositol 3-phosphate [PI(3)P] levels and increased TLR9 endosomal localization. Pharmacological inhibition of PI(3)P synthesis markedly reduced TLR9-mediated IL-6. Single-cell RNA-sequencing (RNA-seq) revealed altered endocytosis, BANK1, and NF-κB1 expression in PTEN-deficient B cells. Ectopic B cell receptor (BCR) expression on non-inflammatory mb1-cKO B cells restored BANK1 and NF-κB1 expression, enhancing TLR9-mediated IL-6 production. Our study highlights PTEN as a crucial inflammatory checkpoint, regulating TLR9/IL-6 axis by fine-tuning PI(3)P homeostasis. Additionally, BCR downregulation prevents the differentiation of inflammatory B cells in PTEN deficiency.**

## INTRODUCTION

B cell lymphopoiesis, crucial for preventing immune diseases, involves the migration of newly generated immature (IM) B cells to the spleen, where they differentiate into mature B2 B cells, comprising follicular (FO) and marginal zone (MZ) subsets. Following antigen exposure, FO B cells undergo somatic hypermutation and class switch recombination, differentiating into memory B cells or high-affinity antibody-producing plasma cells. In contrast, MZ B cells and fetal liver-derived B1 B cells rapidly produce low-affinity antibodies upon antigen encounter.

Phosphatase and tensin homolog (PTEN), a lipid and protein phosphatase, counteracts PI3K-generated 3-phosphoinositide products.[1–3] Upon B cell receptor (BCR) stimulation, active PI3K produces PI(3,4,5)P3, activating Akt and downstream processes. PTEN deactivates the PI3K-Akt pathway, facilitating the transcription of crucial genes RAG1/2 for immunoglobulin rearrangement and pre-B cell differentiation.[4,5] PTEN loss at the pre-B cell stage disrupts development, triggering apoptosis in autoreactive B cells, opposing negative selection.[6] During maturation, PTEN is essential for eliminating autoreactive B cells through secondary light chain gene recombination.[7] B cell intrinsic PTEN ablation alters B cell subset maturation, reducing FO B cells but increasing MZ B cells and B1a cells.[8–10] PTEN also regulates B cell responsiveness, aiding in activation-induced cytidine deaminase induction for class switch recombination.[9] Overall, PTEN plays crucial roles in B cell development, essential for a protective adaptive immune response.

B cells, beyond antibody production, release cytokines shaping the immune response. B cell-derived IL-6 is crucial for T cell homeostasis,[11] antifungal defense,[12] spontaneous germinal center formation,[13] and autoimmune diseases.[13–17] TLR9, recognizing pathogen-associated molecular patterns like CpG DNA, initiates signaling involving Syk, MyD88, IRAKs, and TRAF6, activating NF-κB and AP-1 for cytokine production.[18,19] In B cells, TLR9 recruits BANK1, a B cell-specific adapter protein known to be involved in the BCR-triggered calcium response, amplifying signaling with MyD88 and TRAF6.[20,21] TLR9 activation phosphorylates p38 kinase, enhancing IL-6 translation via the MNK1/2-eIF4E axis.[22] BCR engagement boosts TLR9 activation, promoting its recruitment to autophagosome-like compartments, intensifying innate immune responses.[23]

Conditional PTEN deletion in T cells disrupted immune tolerance in mice, while myeloid PTEN deficiency worsened renal inflammation and liver injury.[24–26] However, genetic ablation of PTEN in B cells did not result in B cell lymphoma or autoimmune phenotypes.[8,27] We thus speculated that the mechanism described earlier elucidates PTEN's roles during B cell development may not apply to mature B cells with PTEN mutations. To explore PTEN's role in mature B cells, we examined mice with CD23-cre-mediated PTEN deletion (CD23-cKO),[28]

[1]Immunology Research Center, National Health Research Institutes, Zhunan Town, Miaoli County 350401, Taiwan
[2]National Institute of Cancer Research, National Health Research Institutes, Zhunan Town, Miaoli County 350401, Taiwan
[3]National Institute of Infectious Diseases and Vaccinology, National Health Research Institutes, Zhunan Town, Miaoli County 350401, Taiwan
[4]Lead contact
*Correspondence: yuwensu@nhri.edu.tw
https://doi.org/10.1016/j.isci.2024.110388

simulating somatic PTEN mutations. PTEN deficiency in mature B2 B cells led to PI(3)P accumulation, facilitating TLR9 signalosome endosomal recruitment. In contrast, B2 B cells from mb1-cre-mediated PTEN deletion (mb1-cKO), which underwent developmental checkpoints in the bone marrow, did not display inflammatory features upon TLR9 engagement due to BCR downregulation. Enforced BCR expression on mb1-cKO B cells strongly induced TLR9-mediated IL-6. The study underscores distinct outcomes of PTEN deficiency in CD23-cKO (somatic mutations) versus mb1-cKO (germline mutations) mice, suggesting that PTEN loss in mature B cells activates the TLR9/IL-6 axis with functional BCR signaling.

## RESULTS

### Ablation of PTEN in mature B cells led to early death in mice

To study the physiological effects of PTEN deletion specifically in peripheral B cells, we bred PTEN$^{F/F}$ mice[29] with CD23-cre mice[28] to generate CD23-cre-PTEN$^{F/F}$ conditional knockout (CD23-cKO) mutant animals. In addition, to delete PTEN beginning at the pro-B cell stage, we generated mb1-cre-PTEN$^{F/F}$ (mb1-cKO) mice. We first determined the efficiency of PTEN deletion in IM (B220$^{+}$CD21$^{low}$CD23$^{low}$IgM$^{+}$), FO (B220$^{+}$CD23$^{hi}$CD21$^{low}$), MZ (B220$^{+}$CD21$^{hi}$CD23$^{low}$), and B1a (B220$^{+}$CD5$^{+}$) B cells in CD23-cKO mice. PTEN deletion efficiency was close to complete (98–100%) in CD23-cKO FO and MZ B cells but occurred in only 46–50% of CD23-cKO IM and B1a B cells (Figures S1A–S1D). Thus, CD23-cKO mice appeared suitable as a model for studying PTEN-deficient mature B2 B cells.

In line with prior findings, PTEN deficiency in CD23-cKO and mb1-cKO mice increased MZ B cells but decreased FO B cells[8,9] (Figures 1A, 1B, S2A, and S2B). CD23-cKO mice aged 8–12 weeks showed spleen enlargement and increased B cell numbers (Figures 1C and 1D). Conversely, mb1-cKO mice had fewer peripheral B cells and a smaller spleen than mb1-control mice (Figures S2C and S2D). We verified that the sharp B cell decrease in mb1-cKO mice resulted from a severe early B cell development block in the bone marrow[30] (Figures S2E and S2F). Notably, 85% of mb1-cKO mice survived over a year due to immunodeficiency (Figure S2G), whereas CD23-cKO mice had a median survival of just 24 weeks, with initial deaths at 12 weeks (Figure 1E). Sick CD23-cKO mice often showed splenomegaly but not lymphadenopathy (Figure 1F). Splenocyte numbers were significantly increased in CD23-cKO mice older than (>) 16 weeks, resulting in an enlarged B cell pool (Figure 1G, left panel). Nevertheless, B cell malignancy was excluded as a cause of death in CD23-cKO mice because the B cell compartment was only slightly expanded in aged mice (Figure 1G, right panel). In CD23-cKO mice at either 8–12 weeks or >16 weeks, serum IgM levels matched those of controls (Figure 1H, left panel). IgG1 levels were significantly reduced due to class switch impairment in PTEN-deficient B cells[9] (Figure 1H, left second panel). Furthermore, anti-nuclear and anti-double stranded DNA (dsDNA) autoantibody levels were not elevated in CD23-cKO mice (Figure 1H, left third and right panels).

The aforementioned findings ruled out antibody-mediated autoimmune disease in CD23-cKO mice. We isolated double-positive (DP) and CD4$^{+}$/CD8$^{+}$ single-positive (SP) thymocytes from both CD23-cKO and control mice at 6 weeks to investigate unexpected PTEN deletion. Reverse-transcription PCR (RT-PCR) analysis confirmed intact PTEN genes in those thymocyte types in both mouse groups (Figure S1E), suggesting that CD23-cKO mice develop an antibody-independent disorder causing premature death.

### Loss of PTEN aberrantly promoted TLR9-mediated IL-6 in B2 B cells

To investigate the impact of CpG stimulation alongside adaptive stimuli on B cell IL-6 production, we examined CpG combined with anti-IgM and anti-CD40 (IgM/CD40) stimulation in freshly sorted FO and MZ B cells. While TLR9-mediated IL-6 production in FO B cells from CD23-cKO and control mice remained unchanged with IgM/CD40 stimulation (Figure S5C), MZ B cells from both CD23-cKO and control mice released more IL-6 with CpG combined with IgM/CD40 stimulation compared to CpG stimulation alone, indicating an additive effect of CpG stimulation combined with adaptive stimuli. We observed modest but significant numbers of B cells infiltrated in the lungs of CD23-cKO mice at 8–12 weeks (Figure S3A), indicating that CD23-cKO mice developed respiratory distress syndrome shortly before death. In CD23-cKO mice older than 16 weeks, lung- and liver-infiltrated T cells seemed to be elevated without statistical significance (Figures S3A and S3B). Immunohistochemistry (IHC) staining with anti-CD4 revealed that CD4$^{+}$ cells were strongly accumulated in the lungs and livers of CD23-cKO mice (Figures S3C and S3D). Furthermore, the levels of GOT and GPT, biomarkers indicating liver injury, were significantly elevated in mutant mice older than 16 weeks (Figure S3E). These results suggest that tissue-infiltrating immune cells play a role in accelerating inflammatory syndrome. In addition, B cell infiltration in vital organs of CD23-cKO mice occurred early, preceding T cell infiltration, while T cells gradually expanded in CD23-cKO mice with age.

To address whether the systemic inflammation in CD23-cKO mice was associated with aberrant myeloid cell homeostasis, we analyzed myeloid cell populations in the spleens and lymph nodes of mice aged 8 weeks and older than 16 weeks using flow cytometry. The gating strategy to analyze myeloid cells is illustrated in Figure S4A. In brief, we sequentially gated CD11b$^{+}$Ly6G$^{+}$ neutrophils, F4/80$^{+}$ macrophages, F4/80$^{+}$MHCII$^{low}$ M1 macrophages, Ly6C$^{+}$CCR2$^{+}$ inflammatory monocytes, CD11b$^{+}$Ly6C$^{+}$ monocytic MDSCs (m-MDSCs), MHCII$^{high}$CD11c$^{+}$ dendritic cells (DCs), MHCII$^{high}$CD11c$^{+}$CD8$^{+}$ DC1,[31] and MHCII$^{high}$CD11c$^{+}$CD11b$^{+}$Ly6C$^{+}$ DC2 from CD45$^{+}$ viable singlet cells, which were negative for the expression of Thy1, CD3, B220, CD19, and NK1.1 (Figure S4A). Cells excluded from these lineages were defined as "other immune cells." In 8-week-old CD23-cKO mice, the frequencies of neutrophils, macrophages, DC1, DC2, inflammatory monocytes, and m-MDSCs in the lymph nodes were significantly increased compared to control mice (Figure S4B). An increase in DC1 was also observed in the spleens of 8-week-old CD23-cKO mice (Figure S4C). In CD23-cKO mice older than 16 weeks, a trend of sustained increased neutrophils and m-MDSCs was observed without statistical significance (Figures S4B and S4C). In summary, the characterization revealed altered myeloid cell homeostasis in 8-week-old CD23-cKO mice.

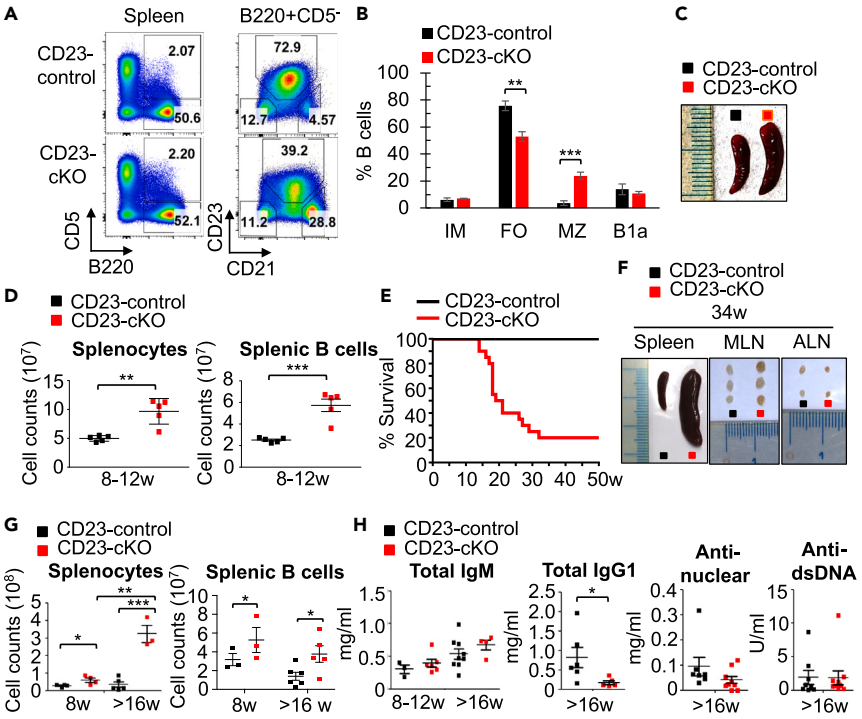


**Figure 1. Ablation of PTEN in mature B cells led to early death in mice**

(A) FACS profiles of B220 versus CD5 in gated lymphocytes (left), and CD21 versus CD23 in CD5$^+$-gated B cells (right), from the spleens of CD23-control and CD23-cKO mice at 8–12 weeks of age.

(B) Histograms showing the percentages of IM, FO, MZ, and B1a B cells in spleens from mice in (A) ($n$ = 3 male plus 2 female mice/group).

(C) Representative images of spleens from the mice in (A).

(D) Cell counts of total splenocytes (left) and splenic B cells (right) from the mice in (A).

(E) Kaplan-Meier curves of female CD23-cKO ($n$ = 20) and female CD23-control ($n$ = 15) mice.

(F) Representative images of spleens, mesenteric lymph nodes (MLNs), and axillary lymph nodes (ALNs) resected from the indicated mice at 34 weeks.

(G) Cell counts of splenocytes (left) and splenic B cells (right) in the indicated mice ($n$ = 3–6 male mice/group) at 8 weeks or >16 weeks.

(H) Levels of total IgM, total IgG1, and anti-nuclear and anti-dsDNA antibodies in the serum of the indicated mice ($n$ = 3–12 male mice/group) at 8–12 weeks or >16 weeks determined by ELISA. The samples were compared using unpaired two-tailed t test; *, $p < 0.05$; **, $p < 0.005$; ***, $p < 0.0005$, and data are presented as mean ± SEM.

To investigate whether mutant B cells contributed to systemic inflammation through the production of proinflammatory cytokines, we assessed the production of IL-6, IL-9, IL-17, CCL5, G-CSF, IL-4, IL-10, IFN-γ, and TNF-α by CD23-cKO B cells in their resting state or upon stimulation with various stimuli: TLR9 agonist CpG, TLR4 agonist LPS, PMA plus ionomycin (P+I), CpG+P+I, or LPS+P+I for 24 h. Cytokine release was detected by intracellular staining. We observed an increase in IL-6 production upon CpG+P+I stimulation and an elevated amount of TNF-α upon P+I stimulation in CD23-cKO B cells (Figure 2A). In the resting state, IL-6 produced by splenic B cells from CD23-cKO mice was slightly but significantly higher than that in control mice (Figures 2B and 2C). The increased IL-6 production occurred in both FO and MZ B cells from CD23-cKO mice after stimulation with CpG for 24 h but was less apparent in B cells stimulated with LPS and not detected in B cells stimulated with CL307 or poly (I:C) (Figure 2D). The addition of the MyD88 inhibitor significantly suppressed TLR9-mediated IL-6 production by B cells from CD23-cKO mice (Figure S5A). The increased TNF-α production by both PTEN-deficient FO and MZ B cells upon CpG stimulation was also confirmed by TNF-α ELISA (Figure S5B). To investigate the impact of CpG stimulation alongside adaptive stimuli on IL-6 production, we examined CpG combined with anti-IgM and anti-CD40 (IgM/CD40) stimulation in freshly sorted FO and MZ B cells. While TLR9-mediated IL-6 production in FO B cells from CD23-cKO and control mice remained unchanged with IgM/CD40 stimulation (Figure S5C), MZ B cells from both CD23-cKO and control mice released more IL-6 with CpG combined with IgM/CD40 stimulation compared to CpG stimulation alone, indicating an additive effect of CpG stimulation combined with adaptive stimuli. To explore PTEN's effect on TLR9-mediated IL-6 production in B1a B cells, we sorted peritoneal B1a B cells from both control and CD23-cKO mice, cultured them with or without CpG stimulation for 24 h, and conducted ELISA. Surprisingly, peritoneal B1a B cells from both groups produced similar IL-6 levels (Figure 2E). These results collectively indicate that PTEN deficiency predominantly affects TLR9-mediated IL-6 production in B2 B cells, suggesting a role for these mutant B cells in driving systemic inflammation.

We also examined the impact of PTEN deficiency in FO and MZ B cells from mb1-cKO mice. The results showed that FO and MZ B cells from mb1-cKO mice produced equal amounts of IL-6 upon CpG stimulation compared to mb1-control cells (Figure S2H). Thus, PTEN

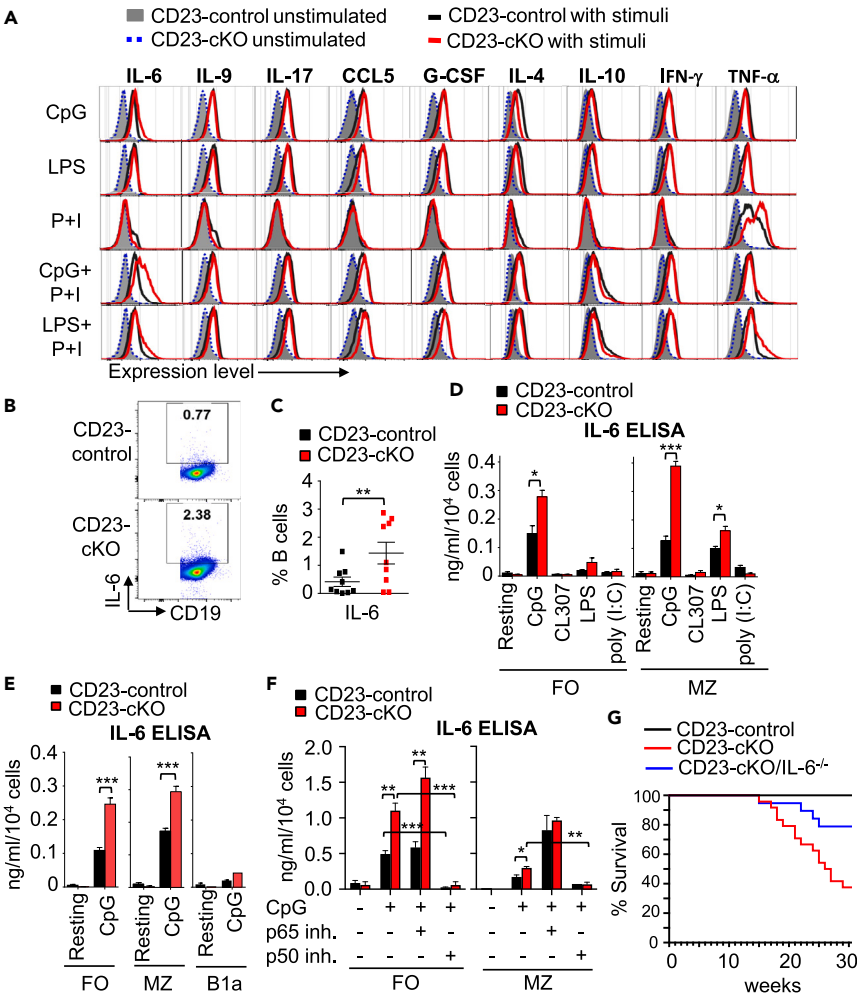


**Figure 2. Loss of PTEN in B2 B cells promotes TLR9-mediated IL-6 production**

(A) Overlaid curves showing the expression levels of IL-6, IL-9, IL-17, CCL5, G-CSF, IL-4, IL-10, IFN-γ, and TNF-α in splenic B cells from the indicated mice ($n$ = 3 male mice/group) at 25–33 weeks was determined by flow cytometry. Cells were left unstimulated or stimulated with CpG, LPS, P+I, CpG+P+I, or LPS+P+I, *in vitro* for 24 h.

(B) FACS profiles of IL-6 versus CD19 in splenic B cells from the indicated mice ($n$ = 9 male mice/group) at 10 w.

(C) Percentages of IL-6$^+$ B cells in splenic B cells as described in (B).

(D) Histograms showing IL-6 produced by FO (left) and MZ (right) B cells, which were left unstimulated (resting) or stimulated with CpG, CL307, LPS, and poly(I:C) *in vitro* for 24 h, as determined by ELISA. Each group containing 3 male mice.

(E) Histograms showing IL-6 produced by FO (left), MZ (middle), and B1a (right) B cells from the indicated mice that were left untreated (resting) or stimulated with CpG *in vitro* for 24 h, as determined by ELISA. Each group containing 4 male mice.

(F) Histograms showing IL-6 produced by FO (left) and MZ (right) B cells, which were left untreated (resting) or stimulated with CpG in the absence or presence of inhibitors (inh.) targeting NF-κB p65 or p50, respectively, for 24 h, as determined by ELISA. Each group containing 4 male mice.

(G) Kaplan-Meier curves of female CD23-control mice (black line, $n$ = 16), female CD23-cKO mice (red line, $n$ = 24), and female CD23-cKO/IL-6$^{-/-}$ double knockout mice (blue line, $n$ = 19). The samples were compared using an unpaired two-tailed t test; *, $p < 0.05$; **, $p < 0.005$; ***, $p < 0.0005$, and the data are presented as mean ± SEM.

deficiency specifically affects TLR9-mediated IL-6 production in B2 B cells from CD23-cKO mice, while it does not significantly impact B1a B cells or FO/MZ B cells from mb1-cKO mice. To dissect TLR9/IL-6 signaling in PTEN-deficient mature B cells, experiments were conducted in freshly sorted FO and MZ B cells from control and CD23-cKO mice, which were stimulated with CpG *in vitro* for 24 h in the presence of inhibitors that block the NF-κB subunits p65/RelA or p50. Inhibition of NF-κB p50, but not p65, strongly blocked TLR9-mediated IL-6 production in all B cells (Figure 2F). These findings highlight the specificity of PTEN's role in regulating TLR9-mediated IL-6 pathway in B2 B cells, which requires NF-κB p50 activity.

To determine if serum IL-6 was influenced by increased IL-6 from PTEN-deficient B cells, we conducted an IL-6 ELISA assay on mouse serum. No significant difference in serum IL-6 was observed between CD23-cKO mice and controls at 8–12 weeks. However, a slight but

significant increase was seen in sick CD23-cKO mice older than 16 weeks (Figure S5D, left panel). Serum TNF-α levels were similar between CD23-cKO mice and controls at 8–12 weeks but increased in older CD23-cKO mice (Figure S5D, right panel). Overall, the data indicate that the loss of PTEN sensitizes FO and MZ B cells' innate response, leading to increased cytokine production, including IL-6 and TNF-α. We bred CD23-cKO mice with IL-6 knockout (IL-$6^{-/-}$) mice to compared the survival rate between CD23-cKO mice and double knockout mice and found a partial rescue of the viability of double knockout mice (Figure 2G). The aforementioned findings implied that IL-6 produced by PTEN-deficient B cells contributed to the systemic inflammation. Despite this, a role of TNF-α produced by PTEN-deficient B cells for the systemic inflammation should not be neglected.

In addition to releasing cytokines, activated B cells also function as antigen-presenting cells, aiding in the activation of the adaptive immune response. To investigate the impact of PTEN deficiency on B cell activation, we sorted FO, MZ, and B1a B cells from both CD23-cKO and control mice. These cells were either left unstimulated (resting) or stimulated with CpG or LPS, representing innate stimuli, as well as CpG plus anti-IgM (CpG+IgM) or anti-IgM plus anti-CD40 (IgM+CD40), which mimic adaptive activation. After culturing the cells in 10% FBS/RPMI medium for 24 h, we analyzed the expression of CD69, CD86, CD80, and MHCII using flow cytometry. Upon CpG stimulation, PTEN-deficient FO, MZ, and B1a B cells showed significantly higher levels of upregulated CD69 compared to controls (Figures S6A–S6F). Additionally, PTEN-deficient MZ and B1a B cells exhibited increased CD86 expression upon CpG stimulation. Hyperactivation of PTEN-deficient B cells upon LPS stimulation was evident through higher levels of CD86 and MHCII specifically in FO B cells. Furthermore, CpG+IgM stimulation led to higher CD69 levels in PTEN-deficient FO and MZ B cells, while IgM+CD40 stimulation resulted in increased CD86 levels in PTEN-deficient FO and MZ B cells. Remarkably, PTEN-deficient FO, MZ, and B1a B cells consistently expressed higher levels of CD80 and MHCII in the resting state. Overall, these findings suggest that PTEN deficiency accelerates the antigen-presenting function of all B cell subsets, thereby contributing to their interaction with the immune system and systemic inflammation.

## PTEN deletion in B2 B cells resulted in PI(3)P accumulation and enhanced TLR9 endosomal localization

Although we demonstrated that the elevation of TLR9-induced IL-6 in PTEN-deficient B cells relied on the activities of NF-κB1 and MyD88 (Figures 2F and S5A), it remained unclear whether PTEN deficiency in B cells impacted the TLR9/MyD88/NF-κB1 axis. Activation of the NF-κB1 pathway requires the phosphorylation of the inhibitor of kappa B kinase (IKK) complex. It has also been shown that IKKβ plays an essential role in the activation and phosphorylation of NF-κB RelA/p65 at S536 (equivalent to murine S534).[32] We examined the dynamic phosphorylation of phosphorylated IKKα/β (p-IKKα/β) at S176/180 and phosphorylated p65 (p-p65) S536 in B cells from both mice upon CpG stimulation for 1 min and 5 min in the absence or presence of a MyD88 inhibitor by intracellular flow cytometry. In the resting state and upon CpG stimulation for 1 min, FO and MZ B cells from both mice displayed a similar level of p-IKK. However, p-IKK signals decreased upon CpG stimulation for 5 min, reaching levels close to the basal level of p-IKK in B cells treated with a MyD88 inhibitor (Figures S7A and S7B). Analysis of p-p65 signal revealed that p-p65 became stronger in both FO and MZ B cells upon CpG stimulation for 1 min, and the induced p-p65 signals immediately decreased upon stimulation for 5 min (Figures S7C and S7D). As expected, the basal and TLR9-induced p-p65 signals were MyD88-dependent. The analysis suggests that PTEN deficiency in CD23-cKO B cells does not directly impact the TLR9/MyD88/NF-κB1 pathway.

TLR9 is initially synthesized in the ER and subsequently translocated to endosomes or lysosomes upon activation.[33] PI(3)P is a hallmark of endosomes and plays a role in recruiting essential molecules for endocytosis.[34] The increased TLR9 activities caused by PTEN deficiency prompted us to explore whether loss of PTEN promoted the endosomal localization of TLR9. We first determined how PTEN deficiency affected PI(3)P levels in B cells. We isolated splenic B cells from control and CD23-cKO mice, stained them with fluorescence-conjugated anti-PI(3)P and anti-LAMP1 to label endosomes and lysosomes, respectively, and visualized signals using confocal microscopy. As expected, PI(3)P levels were significantly higher in resting CD23-cKO B cells (Figures 3A and 3B). However, LAMP-1 signal levels were comparable between control and CD23-cKO B cells. The increase in PI(3)P level in noninflammatory mb1-cKO B cells was obscured compared to those in mb1-controls (Figures 3C and 3D). We further conducted a proximity ligation assay (PLA) to assess the interaction between TLR9 and PI(3)P in control and CD23-cKO B cells. Notably, CD23-cKO B cells exhibited more proximal signals between TLR9 and PI(3)P than controls (Figures 3E and 3F), indicating that PTEN deficiency accelerated the translocation of TLR9 to endosomes.

To identify the synthesis pathway contributing to abnormal TLR9-mediated IL-6 production, we treated sorted FO or MZ B cells from CD23-cKO and control mice with CpG in the presence of the PIK3C3 inhibitor SAR405 or INPP4 inhibitor bpV(phen) (Figure 3G). The PIK3C3 inhibitor strongly reduced TLR9-mediated IL-6 in FO B cells from both CD23-cKO and control mice, while the INPP4 inhibitor had a minor suppressive effect (Figure 3H, left panel). In MZ B cells, both inhibitors minimally impacted TLR9-mediated IL-6 in CD23-cKO cells and had no effect on control cells (Figure 3H, right panel). These findings suggest that PTEN loss accelerates PI(3)P accumulation and TLR9 endosomal localization. Additionally, inhibiting PI(3)P synthesis with a PIK3C3 inhibitor significantly reduces TLR9-mediated IL-6 in FO B cells.

## Endocytosis pathway predicted by scRNA-seq analysis was essential for TLR9-mediated IL-6

Inhibiting PI(3)P synthesis with a PIK3C3 inhibitor only partially blocked the TLR9/IL-6 pathway in PTEN$^{-/-}$ FO B cells and marginally affected the TLR9/IL-6 loop in MZ B cells. This suggests that other molecular mechanisms caused by PTEN deficiency determine TLR9 activity. To explore additional biological processes uniquely associated with the inflammatory phenotype of CD23-cKO B cells, we performed scRNA-seq using the BD Rhapsody platform. Splenic B cells from CD23-control, CD23-cKO, mb1-control, and mb1-cKO mice were either unstimulated or stimulated with CpG for 2 h to detect early responsive genes upon TLR9 stimulation. As a negative control, the p38 inhibitor SB203580

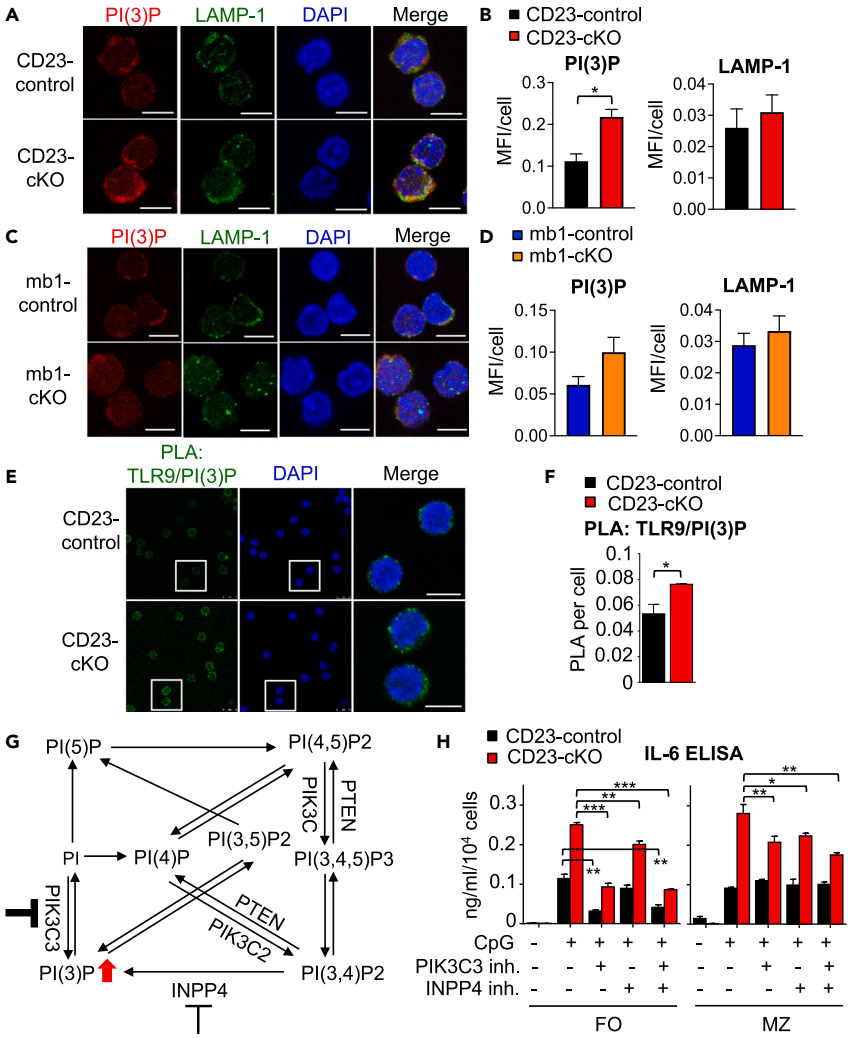


**Figure 3. PTEN deletion in B2 B cells resulted in PI(3)P accumulation and enhanced TLR9 endosomal localization**

(A) Confocal images showing the levels of PI(3)P, LAMP-1, and DAPI in the indicated B cells. Scale bars, 5 μm.

(B) Histograms showing the intensity of PI(3)P and LAMP-1 in the indicated B cells calculated using the mean fluorescence intensity (MFI) from 36 to 186 individual cells per group as described in (A).

(C) Confocal images showing the levels of PI(3)P, LAMP-1, and DAPI in the indicated B cells. Scale bars, 5 μm.

(D) Histograms showing the intensity of PI(3)P and LAMP-1 in the indicated B cells calculated using MFI from 56 individual cells per group as described in (C).

(E) Confocal images showing the interaction between TLR9 and PI(3)P by PLA in the indicated B cells. Scale bars, 5 μm.

(F) Histogram showing the quantified PLA signals of TLR9/PI(3)P in the indicated B cells calculated from 35 to 42 individual cells per group as described in (E).

(G) A diagram illustrating phosphatidylinositol signaling regulated by PI3K and lipid phosphatases. The accumulation of PI(3)P in PTEN-deficient B cells is indicated by a red arrow.

(H) Histograms showing IL-6 produced by FO (left) and MZ (middle) B cells from the indicated mice that were left unstimulated or stimulated with CpG in the absence or presence of inhibitors (inh.) targeting PIK3C3 or INPP4 *in vitro* for 24 h, as determined by ELISA. Each group containing 4 male mice. The samples were compared using an unpaired two-tailed t test; *, $p < 0.05$; **, $p < 0.005$; ***, $p < 0.0005$, and the data are presented as mean ± SEM.

blocked sequential effects mediated by IL-6 (Figure 4A). Among 16,871 cells containing 12 groups that passed quality control, 20,932 genes were detected. Gene set enrichment analysis (GSEA) of pathways in CD23-cKO-CpG versus CD23-control-CpG, mb1-control-CpG, and mb1-cKO-CpG revealed 21 upregulated and 16 downregulated pathways. Upregulated hallmarks included Myc targets, oxidative phosphorylation, heme metabolism, PI3K/AKT/mTOR signaling, protein translation, fatty acid and cholesterol metabolism, oxidative phosphorylation and glycolysis, and allograft rejection (Figure 4B). MSigDB KEGG analysis detected 28 upregulated and 10 downregulated pathways in CpG-stimulated CD23-cKO B cells (Figure 4C). Notably, upregulated pathways included the DNA sensing pathway and endocytosis, while downregulated pathways included TLR signaling and BCR signaling (Figure 4C). A dot plot of some mentioned pathways in all groups was depicted in Figure 4D.

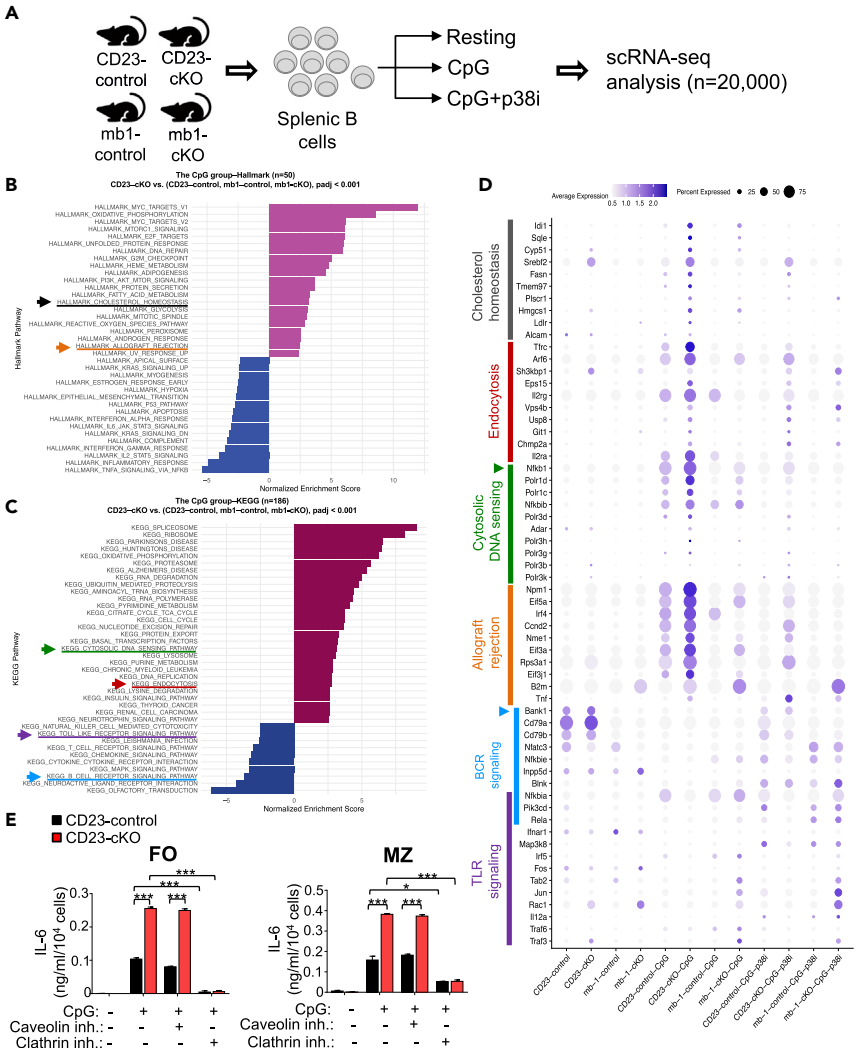


**Figure 4. scRNA-seq analysis revealed that endocytosis was essential for TLR9-mediated IL-6**

(A) A diagram illustrating splenic B cells collected from the four mice strain and the treatments for scRNA-seq analysis.

(B) Hallmark gene sets analysis showing 21 pathways upregulated and 16 pathways downregulated in the CpG-stimulated splenic B cells from CD23-cKO mice.

(C) KEGG database analysis showing 28 pathways upregulated and 10 pathways downregulated in the CpG-stimulated splenic B cells from CD23-cKO mice.

(D) Dotplot analysis showing selected gene clusters from (B) and (C) in B cells in the resting state, upon CpG-stimulation or upon CpG-stimulation in the presence of p38 inhibitor (p38i) from the indicated mice.

(E) Histograms showing IL-6 produced by FO (left) and MZ (right) B cells, which were left unstimulated (–) or stimulated (+) with CpG for 24 h in the absence or presence of inhibitors (inh.) targeting caveolin 1 or clathrin, respectively, as determined by ELISA. Each group containing 2 male and 2 female mice. The samples were compared using an unpaired two-tailed t test; *, $p < 0.05$; **, $p < 0.005$; ***, $p < 0.0005$, and the data are presented as mean ± SEM.

We investigated endocytosis in the aberrant activation of TLR9/IL-6 in PTEN$^{-/-}$ B cells. TLR9, normally in the endoplasmic reticulum (ER), translocates to lysosomes via endocytic vesicles upon CpG stimulation.[35] TLR ligand uptake can occur through clathrin- or caveolin-dependent endocytosis.[36] We purified FO and MZ B cells from CD23-cKO mice, stimulating them with CpG in the absence or presence of clathrin or caveolin 1 inhibitors. After 24 h, IL-6 levels were measured. TLR9-mediated IL-6 in B cells from CD23-cKO and control mice was significantly suppressed by the clathrin inhibitor but not by the caveolin inhibitor (Figure 4E). This effect was consistent in MZ B cells. Overall, these analyses revealed PTEN's crucial role in suppressing TLR9-mediated IL-6 through clathrin-mediated endocytosis. The impact of PTEN deficiency on BANK1 and NF-κB1, along with their significance in the TLR9/IL-6 axis from scRNA-seq analysis, will be addressed later.

## The levels of BANK1 and NF-κB were significantly reduced in mb1-cKO B cells

ScRNA-seq analysis predicted downregulation of BCR signaling and Bank1 mRNA, along with upregulation of NF-κB mRNA in CpG-stimulated CD23-cKO B cells (Figures 4C and 4D). Given the crucial role of BCR in integrating innate and adaptive responses,[37] we hypothesized that the

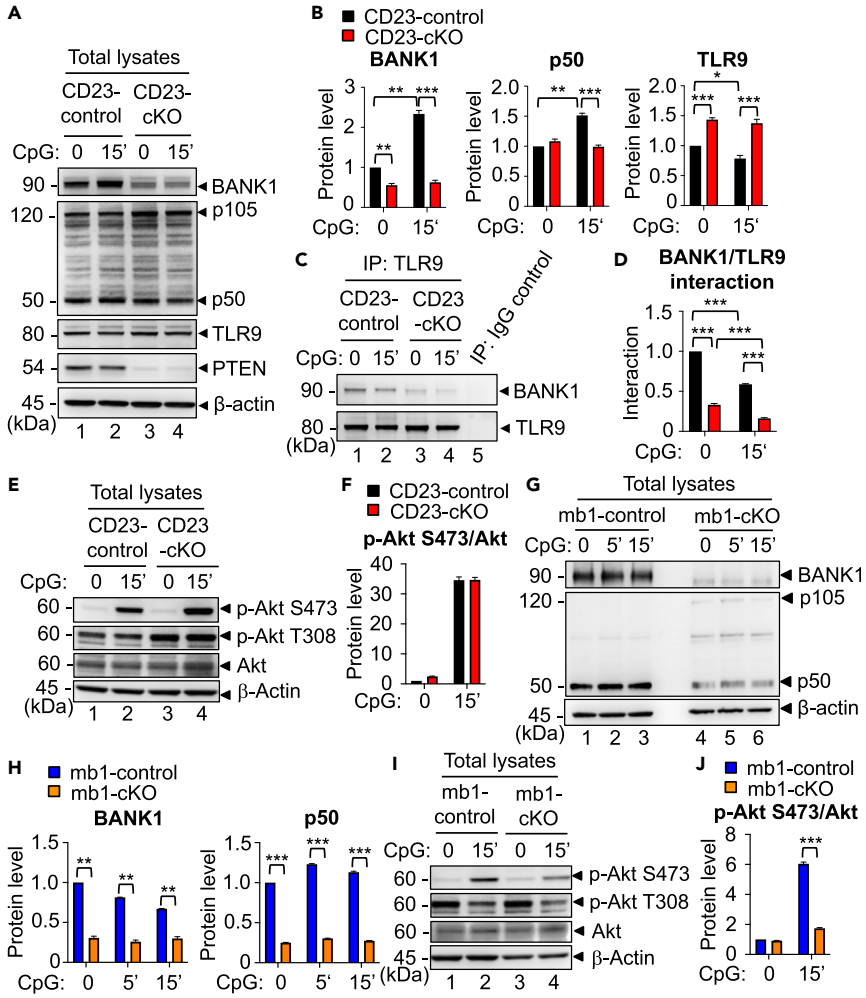


**Figure 5. The levels of BANK1 and NF-κB1 were significantly reduced in non-inflammatory mb1-cKO B cells**

(A) Western blot analyses to show the expression of BANK1, NF-κB1, TLR9, PTEN, and β-actin in splenic B cells from the indicated mice, which were left unstimulated (0) or stimulated with CpG for 15 min. Each group containing 5 male and 5 female mice.

(B) Histograms to show the relative protein levels of BANK1, NF-κB1 p50, and TLR9 in splenic B cells, which were normalized to β-actin, from the indicated mice as described in (A). The expression level of each protein in unstimulated controls was defined as 1.

(C) Immunoprecipitation (IP) with anti-TLR9 combined with BANK1- and TLR9-immunoblots to show the interaction between TLR9 and BANK1 in splenic B cells from the indicated mice, which were left unstimulated (0) or stimulated with CpG for 15 min as described in (A).

(D) Histograms showing the quantification of BANK1 proteins, which were pulled down by anti-TLR9 in B cells as described in (C).

(E) Western blot analyses to show the expression of p-Akt S473, p-Akt T308, Akt, and β-actin in splenic B cells from the indicated mice, which were left unstimulated (0) or stimulated with CpG for 15 min. Each group containing 6–12 female mice.

(F) Histograms showing the relative level of p-Akt S473 in B cells, which was normalized to Akt, as described in (E).

(G) Western blot analyses to show the expression of BANK1, NF-κB1, and β-actin in splenic B cells from the indicated mice, which were left unstimulated (0) or stimulated with CpG for 15 min. Each group containing 3 male mice.

(H) Histograms showing the relative level of BANK1 and NF-κB1 p50 in B cells, which was normalized to β-actin, as described in (G). The levels of BANK1 and NF-κB1 p50 in unstimulated controls were defined as 1.

(I) Western blot analyses to show the expression of p-Akt S473, p-Akt T308, Akt and β-actin in splenic B cells from the indicated mice, which were left unstimulated (0) or stimulated with CpG for 15 min. Each group containing 3 male plus 3 female mice.

(J) Histograms showing the relative level of p-Akt S473 in B cells, which was normalized to Akt, as described in (I). The level of p-Akt S473/Akt in unstimulated controls was defined as 1. The samples were compared using an unpaired two-tailed t test; *, $p < 0.05$; **, $p < 0.005$; ***, $p < 0.0005$, and the data are presented as mean ± SEM.

significance of endocytosis in TLR9/IL-6 pathway might involve both TLR9 and BCR. Since BANK1 participates in both TLR9 and BCR signaling,[20,21] we explored whether elevated TLR9-mediated IL-6 in CD23-cKO B cells was linked to BANK1 expression. BANK1 immunoblotting revealed reduced expression in the steady state and no induction upon CpG stimulation in CD23-cKO B cells, unlike controls (Figures 5A and 5B).

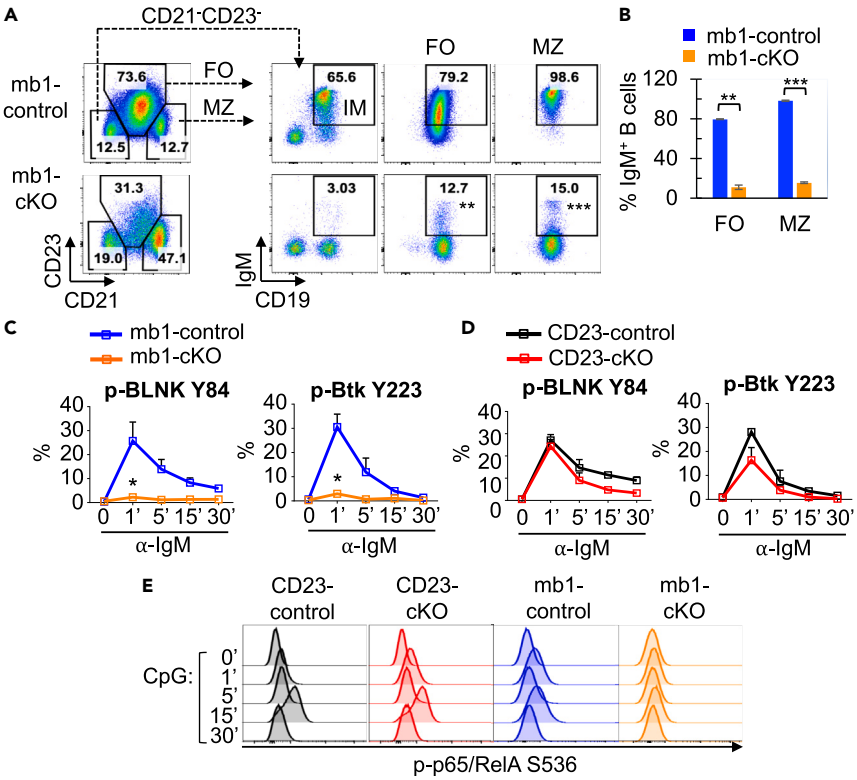


**Figure 6. BCR signaling and TLR9-mediated NF-κB activation were impaired in B2 B cells from mb1-cKO B cells**

(A) FACS profiles of CD21 versus CD23 from B220$^{+}$-gated splenocytes to show the gating of IM, FO, and MZ B cells (left) and FACS profiles of CD19 versus IgM to show IgM expression in those subsets (right) of indicated mice. Data were from 3 independent experiments.

(B) Histograms to show the frequencies of IgM-expressing FO and MZ B cells as described in (A). Each group containing 3 male plus 3 female mice.

(C and D) Curves to show the kinetic induction of BCR-mediated BLNK-phosphorylation (p-BLNK) on Y84 and p-Btk on Y223 in the resting state (0), or upon anti-IgM-stimulation for 1, 5, 15, and 30 min, respectively, from the indicated mice. Each group containing 3 male mice.

(E) Overlaid curves showing p-p65 S536 signals by intracellular staining in splenic B cells from the indicated mice, which were left unstimulated (0) or stimulated with CpG for 1, 5, 15, and 30 min, respectively. Each group containing 3 female mice. The samples were compared using an unpaired two-tailed t test; *, $p < 0.05$; **, $p < 0.005$; ***, $p < 0.0005$, and the data are presented mean ± SEM.

Immunoprecipitation with anti-TLR9 combined with BANK1 immunoblotting in controls showed an interaction between BANK1 and TLR9 in the resting state and upon CpG stimulation. However, this interaction appeared weaker in CD23-cKO B cells (Figures 5C and 5D). In CD23-cKO B cells, the level of TLR9-mediated Akt phosphorylation on S473 seemed unchanged compared to controls (Figures 5E and 5F). These findings suggest that PTEN ablation in mature B cells leads to downregulation of BANK1 and a reduction in the interaction between BANK1 and TLR9.

We then assessed BANK1 expression in non-inflammatory B cells from mb1-cKO mice. Surprisingly, BANK1 protein was markedly reduced in mb1-cKO B cells (Figures 5G and 5H), indicating more severe downregulation compared to CD23-cKO B cells. Additionally, we observed significant decreases in p50 levels in mb1-cKO B cells, along with slight p105 precursor accumulation (Figures 5G and 5H). Furthermore, TLR9-mediated p-Akt S473 signal was significantly reduced in mb1-cKO B cells upon CpG stimulation (Figures 5I and 5J). These data revealed that PTEN loss in mb1-cKO B cells led to more severe downregulation of BANK1 and NF-κB1 p50 proteins than in CD23-cKO B cells, associated with impaired TLR9-mediated Akt S473 phosphorylation.

## BCR signaling and TLR9-mediated NF-κB activation were impaired in B2 B cells from mb1-cKO B cells

In mb1-cKO mice, B cell development was severely blocked in Fr. D in the bone marrow, resulting in reduced egress of IM B cells (Figures S2E and S2F). While FO and MZ B cells were present in the spleen of mb1-cKO mice based on CD23 and CD21 expression, they showed aberrant downregulation of surface IgM and defective IgM-mediated endocytosis (Figures 6A and 6B). Accordingly, BCR-mediated endocytosis was defective in B2 B cells from mb1-cKO mice but normal in B cells from CD23-cKO mice (Figures S5E and S5F). Upon anti-IgM stimulation, splenic B cells from mb1-cKO mice had impaired phosphorylation of BLNK and Btk, unlike CD23-cKO B cells (Figures 6C and 6D). The findings demonstrated that ablation of PTEN downregulated IgM expression and BCR signaling in B2 B cells from mb1-cKO mice. As expected, TLR9-mediated p-p65 at S536 in mb1-cKO B cells was completely diminished, while TLR9-mediated p-p65 occurred normally in CD23-cKO B cells (Figure 6E). In brief, PTEN deficiency in mature B cells mediated by mb1-cre, which undergoes the developmental checkpoint, leads to down-regulation of BCR, impaired BCR-mediated endocytosis, and impaired TLR9-mediated NF-κB activation.

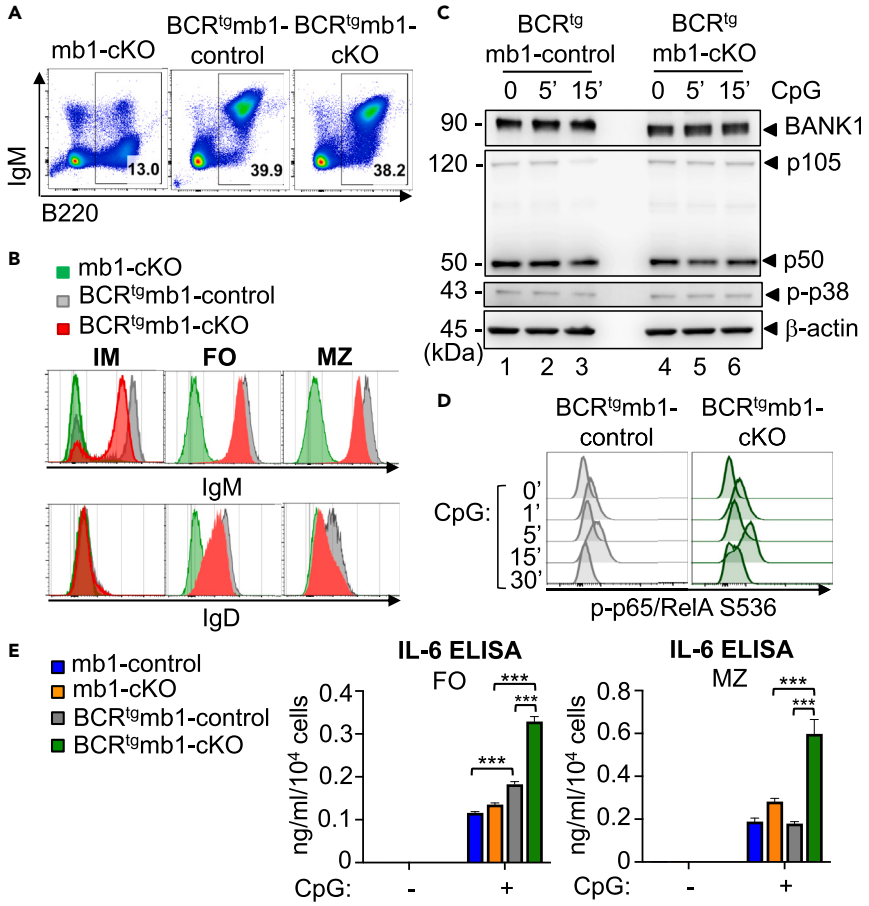


**Figure 7. Ectopic BCR expression in mb1-cKO B cells reconstitutes the expression of BANK1 and NF-κB p50 and elevates TLR9-mediated IL-6 production**

(A) FACS profiles showing the percentages of $B220^+$ splenic B cells from the indicated mice.

(B) Overlaid curves showing levels of surface IgM and IgD in IM, FO, and MZ B cells from the indicated mice.

(C) Western blot analyses to show the expression of BANK1, NF-κB p105 and p50, p-p38, and β-actin, in splenic B cells from the indicated mice, which were left unstimulated (0) or stimulated with CpG for 5 and 15 min. Each group containing 3 male mice.

(D) Overlaid curves showing p-p65 S536 signals by intracellular staining in splenic B cells from the indicated mice, which were left unstimulated (0) or stimulated with CpG for 1, 5, 15, and 30 min. Each group containing 3 male mice.

(E) Histograms showing IL-6 produced by FO (left) and MZ (right) B cells from the indicated mice, which were left unstimulated (–) or stimulated with CpG for 24 h, as determined by ELISA. Each group containing 3 male mice. The samples were compared using an unpaired two-tailed t test; *, $p < 0.05$; **, $p < 0.005$; ***, $p < 0.0005$, and the data are presented mean ± SEM.

## Ectopic BCR expression in mb1-cKO B cells reconstitutes the expression of BANK1 and NF-κB p50 and elevates TLR9-mediated IL-6 production

To explore BCR's role in the TLR response and confirm our hypothesis that mb1-cKO B cells reduce BCR expression to limit TLR9-mediated inflammation, we bred BCR-transgenic (BCRtg) mice with mb1-cKO and mb1-control mice, using HEL-specific BCRtg mice. Flow cytometry in these mice revealed that BCR-transgenic expression restored the $B220^+$ splenic compartment (Figure 7A). Although surface IgM and IgD expression on FO and MZ B cells from BCRtg mb1-cKO mice were largely rescued, the levels remained slightly lower than those on BCRtg mb1-control (Figure 7B). We isolated splenic B cells from BCRtg mb1-cKO and BCRtg mb1-control mice, left them unstimulated or stimulated with CpG for 5 or 15 min, and performed immunoblotting on cellular lysates to detect the expression of BANK and NF-κB p50 proteins. Intriguingly, the levels of BANK1 and NF-κB p50 were almost restored to the levels in BCRtg mb1-controls (Figure 7C). Upon CpG stimulation, the kinetics of p-p65 S536 signals in BCRtg mb1-cKO B cells reverted to the normal levels observed in BCRtg mb1-controls (Figure 7D), suggesting that the enforced expression of BCR restored TLR9-induced NF-κB1 activation in BCRtg mb1-cKO B cells.

Finally, we investigated the role of enforced BCR expression in TLR9-mediated IL-6. We sorted FO and MZ B cells from BCRtg mb1-cKO and BCRtg mb1-control mice, stimulated them with CpG for 24 h, and measured IL-6 levels in the supernatants. Compared to BCRtg mb1-control mice, both FO and MZ B cells from BCRtg mb1-cKO mice exhibited excessive IL-6 production upon CpG stimulation (Figure 7E).

These results confirmed that PTEN deficiency in mature B2 cells from mb1-cKO mice attenuated the TLR9 response by downregulating the protein expression of BCR, BANK1, and NF-κB1.

In summary, our findings underscore PTEN's crucial role in regulating PI(3)P and modulating TLR9 activity, influencing its endosomal trafficking in peripheral B cells. With tonic BCR signaling, endosomal TLR9 activates BANK1 and NF-κB1, leading to increased IL-6 production. Conversely, PTEN deficiency from early developmental stage restrains B cell's TLR9-mediated innate responses by downregulating BCR, BANK1, and NF-κB1. Our data highlight PTEN's significance in peripheral B cells, suppressing TLR9-induced inflammation through coordinated TLR9 and BCR signaling-related lipid homeostasis.

## DISCUSSION

Our study reveals PTEN as a key regulator, preventing hyperactivation of TLR9/IL-6 signaling in B cells. CD23-cKO mice exhibit systemic inflammation with immune cell infiltration in vital organs, not seen in mb1-cKO mice. The abnormal induction of the TLR9/IL-6 axis by PTEN-deficient B cells persistently affects various immune cell types, ultimately promoting systemic inflammation.

In contrast, early PTEN deletion in B-cell lymphopoiesis obstructs development, reducing mature B cell production in mb1-cKO mice. Residual PTEN-deficient peripheral B cells in mb1-cKO mice downregulate BCR and BCR endocytosis. Despite comparable IL-6 production capacity to controls, the downregulation of BCR suggests a beneficial role in controlling innate receptor-mediated inflammation.

While TLR4 activation can induce IL-6 production in B cells, PTEN deficiency specifically affects TLR9/IL-6 signaling in our data. In the resting state, TLR9 resides in the ER and engages in sequential endosomal shuttling, translocating from the ER to the endosome and finally to the lysosome.[38,39] TLR9 signaling initiation depends on PI(3)P in the endosomal lipid domain, crucial for protein trafficking and lysosome maturation.[40,41] Interestingly, TLR4 initiation occurs on the plasma membrane, where PI(4,5)P2 mediates signaling molecule binding.[42] Despite PTEN loss leading to PI(3,4)P2 accumulation, which promotes PI(3)P formation through INPP4B,[43] treatment of PTEN-deficient B cells with an INPP4 inhibitor does not significantly reduce TLR9-mediated IL-6 production. This underscores the essential role of the PIK3C3-PI(3)P-TLR9 pathway in IL-6 production.

In contrast to TLR9 signaling in myeloid cells, TLR9 signaling in B cells is uniquely regulated involving BCR internalization.[23] PTEN-deficient B cells exhibit downregulation of BANK1 protein in both inflammatory and non-inflammatory contexts, suggesting a feedback regulation between PTEN and BANK1. BANK1 positively influences BCR-mediated calcium response and TLR9 signaling transductio and also owns the regulatory role in CD40-mediated Akt activation[44] and type I IFN response in human B cells.[45] The reduced BANK1 expression by PTEN deficiency may have multifaceted effects on B cell activity. Enforcing BCR expression in non-inflammatory PTEN-deficient B cells restores BANK1 expression, indicating stabilization by BCR signaling. The residual BANK1 in inflammatory PTEN-deficient B cells seems sufficient for activating endosomal TLR9. We propose that PTEN deficiency accelerates TLR9 activity by expediting its endosomal trafficking and BANK1 recruitment. Conversely, marked reductions in BANK1, NF-κB1, and BCR proximal signaling in non-inflammatory mb1-cKO B cells reduce innate activity. Restoring BCR expression in mb1-cKO B cells reinstates regular BANK1 and NF-κB1 expression, intensifying abnormal TLR9-mediated IL-6 induction. This suggests that BCR downregulation in mb1-cKO B cells acts as a protective mechanism against hyperactivation of TLR9 signaling. Our study reveals PTEN as both a tumor suppressor and an "inflammation suppressor" restraining TLR9-mediated inflammation by B2 B cells. Downregulation of BCR effectively suppresses innate receptor-driven inflammation induced by PTEN mutation, emphasizing the significance of B-cell intrinsic PTEN in maintaining peripheral immune tolerance.

### Limitations of the study

In the present study, we demonstrated that PTEN deficiency in mature B cells led to the aberrant activation of TLR9-mediated IL-6, contributing to inflammation. Additionally, we observed that PTEN deficiency in mature B cells not only influenced the TLR9/IL-6 pathway but also affected TLR9-mediated TNF-α and the expression of other chemokines that modulate immune cell migration. Thus, the aberrant TLR9/IL-6 pathway represents only part of the dysregulation in PTEN-deficient B cells. Furthermore, the use of several inhibitors to investigate the molecular mechanism underlying PTEN deficiency might yield unexpected off-target effects.

## STAR★METHODS

Detailed methods are provided in the online version of this paper and include the following:

- KEY RESOURCES TABLE
- RESOURCE AVAILABILITY
  - Lead contact
  - Materials availability
  - Data and code availability
- EXPERIMENTAL MODEL AND STUDY PARTICIPANT DETAILS
  - Animals
- METHOD DETAILS
  - B cell purification and cell culture
  - B-cell purification, cell stimulation and drug treatment *in vitro*
  - ELISA

- Flow cytometry
- Immunofluorescence staining and Duolink proximity ligation assay (PLA)
- Immunoblot assay and immunoprecipitation (IP)
- Single-cell RNA-sequencing (scRNA-seq) and data analysis
- Quantification and statistical analysis

## SUPPLEMENTAL INFORMATION

Supplemental information can be found online at https://doi.org/10.1016/j.isci.2024.110388.

## ACKNOWLEDGMENTS

This work was supported by NHRI intramural funding (IM-110-PP-03 and IM-111-PP-03) and the Ministry of Science and Technology (MOST 106-2320-B-400-014, 108-2320-B-400-016-MY3, 108-2811-B-400-532, 109-2811-B-400-511, and 110-2811-B-400-518). We would like to thank Michael Reth and Roberta Pelanda for sharing mb1-cre mice, Meinrad Busslinger for sharing CD23-cre mice, Zhenyue Hao and Kuo-I Lin for scientific discussion, the Laboratory Animal Center of NHRI for animal care, and the NHRI Core Instrument Center for its cell sorting and image service. The graph abstract shown in the paper was created with BioRender.com.

## AUTHOR CONTRIBUTIONS

P.T., M.C., W.H., P.C., S.L., H.C., and Y.S. performed the experiments and data analyses. Y.S. wrote the manuscript. C.K., W.L., T.C., and G.Y. provided materials and scientific feedback. Y.S. designed and supervised the study.

## DECLARATION OF INTERESTS

The authors declare no competing interests.

Received: February 16, 2024
Revised: May 27, 2024
Accepted: June 24, 2024
Published: June 26, 2024

## REFERENCES

1. Burman, C., and Ktistakis, N.T. (2010). Regulation of autophagy by phosphatidylinositol 3-phosphate. FEBS Lett. *584*, 1302–1312. https://doi.org/10.1016/j.febslet.2010.01.011.
2. Hollander, M.C., Blumenthal, G.M., and Dennis, P.A. (2011). PTEN loss in the continuum of common cancers, rare syndromes and mouse models. Nat. Rev. Cancer *11*, 289–301. https://doi.org/10.1038/nrc3037.
3. Malek, M., Kielkowska, A., Chessa, T., Anderson, K.E., Barneda, D., Pir, P., Nakanishi, H., Eguchi, S., Koizumi, A., Sasaki, J., et al. (2017). PTEN regulates PI(3,4)P2 signaling downstream of class I PI3K. Mol. Cell *68*, 566–580.e10. https://doi.org/10.1016/j.molcel.2017.09.024.
4. Amin, R.H., and Schlissel, M.S. (2008). Foxo1 directly regulates the transcription of recombination-activating genes during B cell development. Nat. Immunol. *9*, 613–622. https://doi.org/10.1038/ni.1612.
5. Dengler, H.S., Baracho, G.V., Omori, S.A., Bruckner, S., Arden, K.C., Castrillon, D.H., DePinho, R.A., and Rickert, R.C. (2008). Distinct functions for the transcription factor Foxo1 at various stages of B cell differentiation. Nat. Immunol. *9*, 1388–1398. https://doi.org/10.1038/ni.1667.
6. Shojaee, S., Chan, L.N., Buchner, M., Cazzaniga, V., Cosgun, K.N., Geng, H., Qiu, Y.H., von Minden, M.D., Ernst, T., Hochhaus, A., et al. (2016). PTEN opposes negative selection and enables oncogenic transformation of pre-B cells. Nat. Med. *22*, 379–387. https://doi.org/10.1038/nm.4062.
7. Setz, C.S., Khadour, A., Renna, V., Iype, J., Gentner, E., He, X., Datta, M., Young, M., Nitschke, L., Wienands, J., et al. (2019). Pten controls B-cell responsiveness and germinal center reaction by regulating the expression of IgD BCR. Embo J. *38*, e100249. https://doi.org/10.15252/embj.2018100249.
8. Anzelon, A.N., Wu, H., and Rickert, R.C. (2003). Pten inactivation alters peripheral B lymphocyte fate and reconstitutes CD19 function. Nat. Immunol. *4*, 287–294. https://doi.org/10.1038/ni892.
9. Suzuki, A., Kaisho, T., Ohishi, M., Tsukio-Yamaguchi, M., Tsubata, T., Koni, P.A., Sasaki, T., Mak, T.W., and Nakano, T. (2003). Critical roles of Pten in B cell homeostasis and immunoglobulin class switch recombination. J. Exp. Med. *197*, 657–667.
10. Matsushita, T., Le Huu, D., Kobayashi, T., Hamaguchi, Y., Hasegawa, M., Naka, K., Hirao, A., Muramatsu, M., Takehara, K., and Fujimoto, M. (2016). A novel splenic B1 regulatory cell subset suppresses allergic disease through phosphatidylinositol 3-kinase–Akt pathway activation. J. Allergy Clin. Immunol. *138*, 1170–1182.e9. https://doi.org/10.1016/j.jaci.2015.12.1319.
11. Hasgur, S., Fan, R., Zwick, D.B., Fairchild, R.L., and Valujskikh, A. (2020). B cell-derived IL-1β and IL-6 drive T cell reconstitution following lymphoablation. Am. J. Transplant. *20*, 2740–2754. https://doi.org/10.1111/ajt.15960.
12. Ferreira-Gomes, M., Wich, M., Böde, S., Hube, B., Jacobsen, I.D., and Jungnickel, B. (2021). B Cell Recognition of Candida albicans Hyphae via TLR 2 Promotes IgG1 and IL-6 Secretion for T(H)17 Differentiation. Front. Immunol. *12*, 698849. https://doi.org/10.3389/fimmu.2021.698849.
13. Arkatkar, T., Du, S.W., Jacobs, H.M., Dam, E.M., Hou, B., Buckner, J.H., Rawlings, D.J., and Jackson, S.W. (2017). B cell-derived IL-6 initiates spontaneous germinal center formation during systemic autoimmunity. J. Exp. Med. *214*, 3207–3217. https://doi.org/10.1084/jem.20170580.
14. Barr, T.A., Shen, P., Brown, S., Lampropoulou, V., Roch, T., Lawrie, S., Fan, B., O'Connor, R.A., Anderton, S.M., Bar-Or, A., et al. (2012). B cell depletion therapy ameliorates autoimmune disease through ablation of IL-6-producing B cells. J. Exp. Med. *209*, 1001–1010. https://doi.org/10.1084/jem.20111675.
15. Soni, C., Makita, S., Eichinger, A., Serpas, L., Sisirak, V., and Reizis, B. (2023). Cutting Edge: TLR2 Signaling in B Cells Promotes Autoreactivity to DNA via IL-6 Secretion. J. Immunol. *211*, 1475–1480. https://doi.org/10.4049/jimmunol.2300313.
16. Beesley, C.F., Goldman, N.R., Taher, T.E., Denton, C.P., Abraham, D.J., Mageed, R.A., and Ong, V.H. (2022). Dysregulated B cell function and disease pathogenesis in systemic sclerosis. Front. Immunol. *13*, 999008. https://doi.org/10.3389/fimmu.2022.999008.
17. Graver, J.C., Jiemy, W.F., Altulea, D.H.A., van Sleen, Y., Xu, S., van der Geest, K.S.M., Verstappen, G.M.P.J., Heeringa, P., Abdulahad, W.H., Brouwer, E., et al. (2023).

Cytokine producing B-cells and their capability to polarize macrophages in giant cell arteritis. J. Autoimmun. *140*, 103111. https://doi.org/10.1016/j.jaut.2023.103111.

18. Kremlitzka, M., Mácsik-Valent, B., and Erdei, A. (2015). Syk is indispensable for CpG-induced activation and differentiation of human B cells. Cell. Mol. Life Sci. *72*, 2223–2236. https://doi.org/10.1007/s00018-014-1806-x.
19. Kawai, T., and Akira, S. (2007). Signaling to NF-kappaB by Toll-like receptors. Trends Mol. Med. *13*, 460–469. https://doi.org/10.1016/j.molmed.2007.09.002.
20. Yokoyama, K., Su Ih, I.H., Tezuka, T., Yasuda, T., Mikoshiba, K., Tarakhovsky, A., and Yamamoto, T. (2002). BANK regulates BCR-induced calcium mobilization by promoting tyrosine phosphorylation of IP(3) receptor. EMBO J. *21*, 83–92. https://doi.org/10.1093/emboj/21.1.83.
21. Georg, I., Díaz-Barreiro, A., Morell, M., Pey, A.L., and Alarcón-Riquelme, M.E. (2020). BANK1 interacts with TRAF6 and MyD88 in innate immune signaling in B cells. Cell. Mol. Immunol. *17*, 954–965. https://doi.org/10.1038/s41423-019-0254-9.
22. Wu, Y.-Y., Kumar, R., Haque, M.S., Castillejo-López, C., and Alarcón-Riquelme, M.E. (2013). BANK1 controls CpG-induced IL-6 secretion via a p38 and MNK1/2/eIF4E translation initiation pathway. J. Immunol. *191*, 6110–6116. https://doi.org/10.4049/jimmunol.1301203.
23. Chaturvedi, A., Dorward, D., and Pierce, S.K. (2008). The B Cell Receptor Governs the Subcellular Location of Toll-like Receptor 9 Leading to Hyperresponses to DNA-Containing Antigens. Immunity *28*, 799–809. https://doi.org/10.1016/j.immuni.2008.03.019.
24. Suzuki, A., Yamaguchi, M.T., Ohteki, T., Sasaki, T., Kaisho, T., Kimura, Y., Yoshida, R., Wakeham, A., Higuchi, T., Fukumoto, M., et al. (2001). T cell-specific loss of Pten leads to defects in central and peripheral tolerance. Immunity *14*, 523–534. https://doi.org/10.1016/s1074-7613(01)00134-0.
25. An, C., Jiao, B., Du, H., Tran, M., Zhou, D., and Wang, Y. (2022). Myeloid PTEN deficiency aggravates renal inflammation and fibrosis in angiotensin II-induced hypertension. J. Cell. Physiol. *237*, 983–991. https://doi.org/10.1002/jcp.30574.
26. Yang, T., Qu, X., Zhao, J., Wang, X., Wang, Q., Dai, J., Zhu, C., Li, J., and Jiang, L. (2023). Macrophage PTEN controls STING-induced inflammation and necroptosis through NICD/NRF2 signaling in APAP-induced liver injury. Cell Commun. Signal. *21*, 160. https://doi.org/10.1186/s12964-023-01175-4.
27. Miletic, A.V., Anzelon-Mills, A.N., Mills, D.M., Omori, S.A., Pedersen, I.M., Shin, D.M., Ravetch, J.V., Bolland, S., Morse, H.C., 3rd, and Rickert, R.C. (2010). Coordinate suppression of B cell lymphoma by PTEN and SHIP phosphatases. J. Exp. Med. *207*, 2407–2420. https://doi.org/10.1084/jem.20091962.
28. Kwon, K., Hutter, C., Sun, Q., Bilic, I., Cobaleda, C., Malin, S., and Busslinger, M. (2008). Instructive role of the transcription factor E2A in early B lymphopoiesis and germinal center B cell development. Immunity *28*, 751–762. https://doi.org/10.1016/j.immuni.2008.04.014.
29. Lesche, R., Groszer, M., Gao, J., Wang, Y., Messing, A., Sun, H., Liu, X., and Wu, H. (2002). Cre/loxP-mediated inactivation of the murine Pten tumor suppressor gene. Genesis *32*, 148–149.
30. Lai, M., Gonzalez-Martin, A., Cooper, A.B., Oda, H., Jin, H.Y., Shepherd, J., He, L., Zhu, J., Nemazee, D., and Xiao, C. (2016). Regulation of B-cell development and tolerance by different members of the miR-17∼92 family microRNAs. Nat. Commun. *7*, 12207. https://doi.org/10.1038/ncomms12207.
31. Hongo, D., Zheng, P., Dutt, S., Pawar, R.D., Meyer, E., Engleman, E.G., and Strober, S. (2021). Identification of Two Subsets of Murine DC1 Dendritic Cells That Differ by Surface Phenotype, Gene Expression, and Function. Front. Immunol. *12*, 746469. https://doi.org/10.3389/fimmu.2021.746469.
32. Yang, F., Tang, E., Guan, K., and Wang, C.Y. (2003). IKK beta plays an essential role in the phosphorylation of RelA/p65 on serine 536 induced by lipopolysaccharide. J. Immunol. *170*, 5630–5635. https://doi.org/10.4049/jimmunol.170.11.5630.
33. Lee, B.L., and Barton, G.M. (2014). Trafficking of endosomal Toll-like receptors. Trends Cell Biol. *24*, 360–369. https://doi.org/10.1016/j.tcb.2013.12.002.
34. Raiborg, C., Schink, K.O., and Stenmark, H. (2013). Class III phosphatidylinositol 3-kinase and its catalytic product PtdIns3P in regulation of endocytic membrane traffic. FEBS J. *280*, 2730–2742. https://doi.org/10.1111/febs.12116.
35. Leifer, C.A., Kennedy, M.N., Mazzoni, A., Lee, C., Kruhlak, M.J., and Segal, D.M. (2004). TLR9 is localized in the endoplasmic reticulum prior to stimulation. J. Immunol. *173*, 1179–1183. https://doi.org/10.4049/jimmunol.173.2.1179.
36. Khan, S., Bijker, M.S., Weterings, J.J., Tanke, H.J., Adema, G.J., van Hall, T., Drijfhout, J.W., Melief, C.J.M., Overkleeft, H.S., van der Marel, G.A., et al. (2007). Distinct uptake mechanisms but similar intracellular processing of two different toll-like receptor ligand-peptide conjugates in dendritic cells. J. Biol. Chem. *282*, 21145–21159. https://doi.org/10.1074/jbc.M701705200.
37. Otipoby, K.L., Waisman, A., Derudder, E., Srinivasan, L., Franklin, A., and Rajewsky, K. (2015). The B-cell antigen receptor integrates adaptive and innate immune signals. Proc. Natl. Acad. Sci. USA *112*, 12145–12150. https://doi.org/10.1073/pnas.1516428112.
38. Latz, E., Schoenemeyer, A., Visintin, A., Fitzgerald, K.A., Monks, B.G., Knetter, C.F., Lien, E., Nilsen, N.J., Espevik, T., and Golenbock, D.T. (2004). TLR9 signals after translocating from the ER to CpG DNA in the lysosome. Nat. Immunol. *5*, 190–198. https://doi.org/10.1038/ni1028.
39. Kim, Y.M., Brinkmann, M.M., Paquet, M.E., and Ploegh, H.L. (2008). UNC93B1 delivers nucleotide-sensing toll-like receptors to endolysosomes. Nature *452*, 234–238. https://doi.org/10.1038/nature06726.
40. Bonham, K.S., Orzalli, M.H., Hayashi, K., Wolf, A.I., Glanemann, C., Weninger, W., Iwasaki, A., Knipe, D.M., and Kagan, J.C. (2014). A promiscuous lipid-binding protein diversifies the subcellular sites of toll-like receptor signal transduction. Cell *156*, 705–716. https://doi.org/10.1016/j.cell.2014.01.019.
41. Jeschke, A., Zehethofer, N., Lindner, B., Krupp, J., Schwudke, D., Haneburger, I., Jovic, M., Backer, J.M., Balla, T., Hilbi, H., and Haas, A. (2015). Phosphatidylinositol 4-phosphate and phosphatidylinositol 3-phosphate regulate phagolysosome biogenesis. Proc. Natl. Acad. Sci. USA *112*, 4636–4641. https://doi.org/10.1073/pnas.1423456112.
42. Park, B.S., Song, D.H., Kim, H.M., Choi, B.S., Lee, H., and Lee, J.O. (2009). The structural basis of lipopolysaccharide recognition by the TLR4-MD-2 complex. Nature *458*, 1191–1195. https://doi.org/10.1038/nature07830.
43. Gewinner, C., Wang, Z.C., Richardson, A., Teruya-Feldstein, J., Etemadmoghadam, D., Bowtell, D., Barretina, J., Lin, W.M., Rameh, L., Salmena, L., et al. (2009). Evidence that inositol polyphosphate 4-phosphatase type II is a tumor suppressor that inhibits PI3K signaling. Cancer Cell *16*, 115–125. https://doi.org/10.1016/j.ccr.2009.06.006.
44. Aiba, Y., Yamazaki, T., Okada, T., Gotoh, K., Sanjo, H., Ogata, M., and Kurosaki, T. (2006). BANK negatively regulates Akt activation and subsequent B cell responses. Immunity *24*, 259–268. https://doi.org/10.1016/j.immuni.2006.01.002.
45. Jiang, S.H., Athanasopoulos, V., Ellyard, J.I., Chuah, A., Cappello, J., Cook, A., Prabhu, S.B., Cardenas, J., Gu, J., Stanley, M., et al. (2019). Functional rare and low frequency variants in BLK and BANK1 contribute to human lupus. Nat. Commun. *10*, 2201. https://doi.org/10.1038/s41467-019-10242-9.
46. Hobeika, E., Thiemann, S., Storch, B., Jumaa, H., Nielsen, P.J., Pelanda, R., and Reth, M. (2006). Testing gene function early in the B cell lineage in mb1-cre mice. Proc. Natl. Acad. Sci. USA *103*, 13789–13794. https://doi.org/10.1073/pnas.0605944103.
47. Mason, D.Y., Jones, M., and Goodnow, C.C. (1992). Development and follicular localization of tolerant B lymphocytes in lysozyme/anti-lysozyme IgM/IgD transgenic mice. Int Immunol *4*, 163–175. https://doi.org/10.1093/intimm/4.2.163.
48. Kopf, M., Baumann, H., Freer, G., Freudenberg, M., Lamers, M., Kishimoto, T., Zinkernagel, R., Bluethmann, H., and Kohler, G. (1994). Impaired immune and acute-phase responses in interleukin-6-deficient mice. Nature *368*, 339–342. https://doi.org/10.1038/368339a0.
49. Hao, Y., Hao, S., Andersen-Nissen, E., Mauck, W.M., Zheng, S., Butler, A., Lee, M.J., Wilk, A.J., Darby, C., Zager, M., et al. (2021). Integrated analysis of multimodal single-cell data. Cell *184*, 3573–3587.e29. https://doi.org/10.1016/j.cell.2021.04.048.
50. Akkaya, M., Akkaya, B., Kim, A.S., Miozzo, P., Sohn, H., Pena, M., Roesler, A.S., Theall, B.P., Henke, T., Kabat, J., et al. (2018). Toll-like receptor 9 antagonizes antibody affinity maturation. Nat. Immunol. *19*, 255–266. https://doi.org/10.1038/s41590-018-0052-z.
51. Bolte, S., and Cordelières, F.P. (2006). A guided tour into subcellular colocalization analysis in light microscopy. J. Microsc. *224*, 213–232. https://doi.org/10.1111/j.1365-2818.2006.01706.x.

## STAR★METHODS

### KEY RESOURCES TABLE

| REAGENT or RESOURCE | SOURCE | IDENTIFIER |
|---|---|---|
| Antibodies | | |
| PE anti-mouse Ly-51 Antibody (clone 6C3) | BioLegend | Cat#108307; RRID: AB_313364 |
| Brilliant Violet 510™ anti-mouse CD5 Antibody (clone 53-7.3) | BioLegend | Cat#100627; RRID: AB_2563930 |
| PE-Cyanine7 anti-mouse CD23 Antibody (clone B3B4) | BioLegend | Cat#101614; RRID: AB_2103036 |
| Alexa Fluor® 488 anti-mouse CD24 Antibody (clone M1/69) | BioLegend | Cat#101815; RRID: AB_493483 |
| Pacific Blue™ anti-mouse IgD Antibody (clone 11-26c.2a) | BioLegend | Cat#405712; RRID: AB_1937244 |
| APC anti-mouse IgM Antibody (clone RMM-1) | BioLegend | Cat#406509; RRID: AB_315059 |
| PE anti-mouse CCL5 (RANTES) Antibody (clone 2E9/CCL5) | BioLegend | Cat#149104; RRID: AB_2564406 |
| APC-Cy™7 Rat Anti-Mouse CD45R (clone RA3-6B2) | BD Biosciences | Cat#552094; RRID: AB_394335 |
| APC Hamster Anti-Mouse CD3e (clone 145-2C11) | BD Biosciences | Cat#553066; RRID: AB_398529 |
| BV510 Rat Anti-Mouse CD4 (clone RM4-5) | BD Biosciences | Cat#563106; RRID: AB_2687550 |
| BB515 Rat Anti-Mouse CD8α (clone 53-6.7) | BD Biosciences | Cat#564422; RRID: AB_2738801 |
| BV510 Rat Anti-Mouse CD19 (clone 1D3) | BD Biosciences | Cat#562956; RRID: AB_2737915 |
| PE Rat Anti-Mouse CD21/CD35 (clone 7G6) | BD Biosciences | Cat#552957; RRID: AB_394532 |
| APC Rat Anti-Mouse CD43 (clone S7) | BD Biosciences | Cat#560663; RRID: AB_1727479 |
| Alexa Fluor 488® Mouse anti-BLNK (pY84) (clone J117-1278) | BD Biosciences | Cat#558444; RRID: AB_2064951 |
| BV421 Mouse Anti-Btk (pY223)/Itk (pY180) (clone N35-86) | BD Biosciences | Cat#564848; RRID: AB_2738982 |
| Alexa Fluor 488® Rat Anti-Mouse IFN-γ (clone XMG1.2) | BD Biosciences | Cat#557724; RRID: AB_396832 |
| BV421 Rat Anti-Mouse IL-4 (clone 11B11) | BD Biosciences | Cat#562915; RRID: AB_2737889 |
| Alexa Fluor 488® Rat Anti-Mouse IL-6 (clone MP5-20F3) | BD Biosciences | Cat#561363; RRID: AB_10694253 |
| Alexa Fluor® 647 Armenian Hamster anti-Mouse IL-9 (clone D9302C12) | BD Biosciences | Cat#561464; RRID: AB_10644410 |
| APC Rat Anti-Mouse IL-10 (clone JES5-16E3) | BD Biosciences | Cat#554468; RRID: AB_398558 |
| Alexa Fluor® 488 Rat anti-Mouse IL-17A (clone TC11-18H10) | BD Biosciences | Cat#560220; RRID: AB_1645194 |
| PE Rat Anti-Mouse TNF (clone MP6-XT22) | BD Biosciences | Cat#554419; RRID: AB_395380 |
| Biotin Rat Anti-Mouse CD90.2 (clone 30-H12) | BD Biosciences | Cat#553011; RRID: AB_394549 |
| Biotin Mouse Anti-Mouse NK-1.1 (clone PK136) | BD Biosciences | Cat#553163; RRID: AB_394675 |
| Biotin Rat Anti-Mouse Ly-6G and Ly-6C (clone RB6-8C5) | BD Biosciences | Cat#553125; RRID: AB_394641 |
| Biotin Rat Anti-Mouse CD49b (clone DX5) | BD Biosciences | Cat#553856; RRID: AB_395092 |
| Biotin Rat Anti-CD11b (clone M1/70) | BD Biosciences | Cat#553309; RRID: AB_394773 |
| Biotin Hamster Anti-Mouse CD11c (clone HL3) | BD Biosciences | Cat#553800; RRID: AB_395059 |
| Biotin Rat Anti-Mouse TER-119/Erythroid Cells (clone TER-119) | BD Biosciences | Cat#553672; RRID: AB_104231 |
| PE Rabbit monoclonal anti-phospho-NF-κB p65 (Ser536) (clone 93H1) | Cell Signaling Technology | Cat#5733S; RRID: AB_2313773 |
| Alexa Fluor® 488 Rabbit monoclonal anti-phospho-IKKα/β (Ser176/180) (clone 16A6) | Cell Signaling Technology | Cat#92255S; RRID: AB_2313773 |
| Rabbit monoclonal anti-β-Actin (clone 13E5) | Cell Signaling Technology | Cat#4970S; RRID: AB_2313773 |
| Rabbit monoclonal anti-Akt (clone C67E7) | Cell Signaling Technology | Cat#4691S; RRID: AB_2313773 |
| Rabbit monoclonal anti-phospho-Akt (Thr308) (clone D25E6) | Cell Signaling Technology | Cat#13038S; RRID: AB_2313773 |
| Rabbit polyclonal anti-phospho-Akt (Ser473) | Cell Signaling Technology | Cat#9271S; RRID: AB_2313773 |
| Rabbit monoclonal anti-LAMP1 (clone D2D11) | Cell Signaling Technology | Cat#9091S; RRID: AB_2313773 |

(*Continued on next page*)

*Continued*

| REAGENT or RESOURCE | SOURCE | IDENTIFIER |
|---|---|---|
| Rabbit monoclonal anti-NF-κB1 p105/p50 (clone D7H5M) | Cell Signaling Technology | Cat#12540S; RRID: AB_2313773 |
| Rabbit polyclonal anti-p38α | Cell Signaling Technology | Cat#9218S; RRID: AB_2313773 |
| Rabbit monoclonal anti-phospho-p38 (Thr180/Tyr182) (clone D3F9) | Cell Signaling Technology | Cat#4511S; RRID: AB_2313773 |
| Rabbit monoclonal anti-CD4 (clone D7D2Z) | Cell Signaling Technology | Cat#25229S; RRID: AB_2313773 |
| Mouse monoclonal anti-BANK1 (F-8) | SANTA CRUZ BIOTECHNOLOGY | Cat#sc-393611; RRID: AB_2313773 |
| Rabbit polyclonal anti-Syk (N-19) | SANTA CRUZ BIOTECHNOLOGY | Cat#sc-1077; RRID: AB_2313773 |
| eFluor™ 660 Rat anti-G-CSF (clone 9B4-CSF) | eBioscience | Cat#50-7353-80; RRID: AB_2313773 |
| Rabbit polyclonal anti-TLR9 | Invitrogen | Cat#PA5-20203; RRID: AB_11152135 |
| Alexa Fluor™ 488 Goat anti-Rabbit IgG (H + L) | Invitrogen | Cat#A-11034; RRID: AB_2576217 |
| AffiniPure™ F(ab')$_2$ Fragment Goat Anti-Mouse IgM, μ chain specific | Jackson ImmunoResearch LABORATORIES | Cat#115-006-020; RRID: AB_2338469 |
| Peroxidase AffiniPure™ Goat Anti-Mouse IgG, light chain specific | Jackson ImmunoResearch LABORATORIES | Cat#115-035-174; RRID: AB_2338512 |
| Goat Anti-Mouse IgG1, Human ads-UNLB | SouthernBiotech | Cat#1070-01; RRID: AB_2794408 |
| Goat Anti-Mouse IgM, Human ads-UNLB | SouthernBiotech | Cat#1020-01; RRID: AB_2794197 |
| Mouse monoclonal anti-PtdIns(3)P | Echelon Biosciences | Cat#Z-P003; RRID: AB_2313773 |
| **Chemicals, peptides, and recombinant proteins** | | |
| 7-Aminoactinomycin D (7-AAD) | Sigma-Aldrich | Cat#A9400-1MG; CAS: 7240-37-1 |
| bpV(phen) | Cayman CHEMICAL | Cat#13331; CAS: 171202-16-7 |
| BD GlogiPlug™ Protein Transport Inhibitor (Containing Brefeldin A) | BD Biosciences | Cat#555029 |
| Caffeic acid phenethyl ester (CAPE) | Tocris Biosciences | Cat#2743; CAS: 104594-70-9 |
| BD Cytofix™ Fixation Buffer | BD Biosciences | Cat#554655 |
| ODN 1668 | InvivoGen | Cat#tlrl-1668-1 |
| CL307 | InvivoGen | Cat#tlrl-c307 |
| Poly(I:C) | InvivoGen | Cat#tlrl-pic |
| Immobilon® Western Chemiluminescent HRP Substrate | Miipore | Cat#WBKLS0500 |
| Image-iT™ FX Signal Enhancer | Invitrogen | Cat#I36933 |
| BD IMag™ Streptavidin Particles Plus - DM | BD Biosciences | Cat#557812 |
| Ionomycin | Sigma-Aldrich | Cat#I9657-1MG; CAS: 56092-81-0 |
| Kamebakaurin | MedChemExpress | Cat#HY-N6046; CAS: 73981-34-7 |
| LPS | InvivoGen | Cat#tlrl-3pelps |
| Methyl-β-cyclodextrin | MedChemExpress | Cat#HY-101461; CAS: 128446-36-6 |
| MK-2206 dihydrochloride | MedChemExpress | Cat#HY-10358; CAS: 1032350-13-2 |
| BD GolgiStop™ Protein Transport Inhibitor (Containing Monensin) | BD Biosciences | Cat#554724 |
| PMA | Sigma-Aldrich | Cat#P1585-1MG; CAS: 16561-29-8 |
| SAR405 | MedChemExpress | Cat#HY-124981; CAS: 1523406-39-4 |
| SB203580 | InvivoGen | Cat#inh-sb20-5; CAS: 152121-47-6 |
| RPMI 1640 medium | Gibco | Cat#11875093 |
| GlutaMAX | Gibco | Cat#35050061 |
| Penicillin-streptomycin | Gibco | Cat#15140122 |
| HEPES | Gibco | Cat#1563008 |
| 2-mercaptoethanol | Gibco | Cat#21985023 |
| Fixable Viability Stain 620 | BD Biosciences | Cat#564996; RRID: AB_2869636 |

(*Continued on next page*)

*Continued*

| REAGENT or RESOURCE | SOURCE | IDENTIFIER |
|---|---|---|
| Duolink® *In Situ* PLA® Probe Anti-Rabbit PLUS | Sigma-Aldrich | Cat#DUO92002 |
| Duolink® *In Situ* PLA® Probe Anti-Mouse MINUS | Sigma-Aldrich | Cat#DUO92004 |
| Duolink® *In Situ* Detection Reagent Green | Sigma-Aldrich | Cat#DUO92014 |
| DAPI | Invitrogen | Cat#D1306 |
| ProLong™ Gold Anti-fade Reagent | Invitrogen | Cat#P36930 |
| TJ-M2010-5 | MedChemExpress | Cat#HY-139397; CAS: 1357471-57-8 |
| **Critical commercial assays** | | |
| APEX™ Antibody Labeling Kits (Alexa Fluor™ 555) | Invitrogen | Cat#A10470 |
| BD Pharmingen™ Transcription Factor Buffer Set | BD Biosciences | Cat#562574; RRID: AB_2869424 |
| BD Pharmingen™ Transcription Factor Phospho Buffer Set | BD Biosciences | Cat#563239; RRID: AB_2869473 |
| BODIPY™ 493/503 (4,4-Difluoro-1,3,5,7,8-Pentamethyl-4-Bora-3a,4a-Diaza-s-Indacene) | Invitrogen | Cat#D3922 |
| BD Rhapsody™ Whole Transcriptome Analysis (WTA) Reagent Kit | BD Biosciences | Cat#633802 |
| Mouse anti-dsDNA ELISA Kit | Fujifilm-Wako-Shibayagi | Cat#AKRDD-061 |
| Anti-nuclear antibody (ANA) ELISA kit | antibodies-online | Cat#ABIN772680 |
| Mouse IL-6 DuoSet ELISA | R&D | Cat#DY406-05 |
| Mouse TNF-α DuoSet ELISA | R&D | Cat#DY410-05 |
| **Deposited data** | | |
| Raw and analyzed data | This paper | GEO: GSE179715 |
| **Experimental models: Organisms/strains** | | |
| Mouse: B6.129S4-Pten$^{tm1Hwu}$/J | The Jackson Laboratory[29] | RRID:IMSR_JAX:006440 |
| Mouse: mb1/cre C57BL/6 | Hobeika et al.[46] | N/A |
| Mouse: CD23/cre C57BL/6 | Kwon et al.[28] | N/A |
| Mouse: C57BL/6-Tg(IghelMD4)4Ccg/J | The Jackson Laboratory[47] | RRID:IMSR_JAX:002595 |
| Mouse: B6.129S2-Il6$^{tm1Kopf}$/J | The Jackson Laboratory[48] | RRID:IMSR_JAX:002650 |
| **Oligonucleotides** | | |
| PTEN-P1 (CAAGCACTCTGCGAACTGAGCTAC) | This paper | N/A |
| PTEN-P2 (AATCTAGGGCCTCTTGTGCCTTTAA) | This paper | N/A |
| PTEN-P3 (GCTTGATATCGAATTCCTGCAGC) | This paper | N/A |
| CD14 forward (GCTCAAACTTTCAGAATCTACCGAC) | This paper | N/A |
| CD14 reverse (AGTCAGTTCCTGGAGGCCGGAAATC) | This paper | N/A |
| **Software and algorithms** | | |
| ImageJ | NIH | https://imagej.net |
| FlowJo | BD | https://www.flowjo.com |
| Seven Bridges platform | Seven Bridges Genomics | https://sevenbriges.com |
| Seurat v4.1.0 | Hao et al.[49] | https://github.com/satijalab/seurat |
| GraphPad Prism | GraphPad | https://www.graphpad.com |

## RESOURCE AVAILABILITY

### Lead contact

Further information and requests for resources and reagents should be directed to and will be fulfilled by the lead contact, Yu-Wen Su (yuwensu@nhri.edu.tw).

### Materials availability

All unique/stable reagents generated in this study are available from the lead contact with a completed Materials Transfer Agreement.

### Data and code availability

- Single-cell RNA-seq data derived from mice samples have been deposited at NIH GEO database and is publicly available as of the date of publication. The Access number GSE179715 is listed in the key resources table.
- This study did not report any original code.
- Any additional information required to reanalyze the data reported in this paper is available from the lead contact upon request.

## EXPERIMENTAL MODEL AND STUDY PARTICIPANT DETAILS

### Animals

PTEN$^{F/F}$, HEL-specific BCRtg and IL-6 knockout mice were obtained from the Jackson Laboratory (JAX stock #006440, #002595 and #002650).[29,47,48] The mb1-cre mice[46] were obtained from Michael Reth and Roberta Pelanda at the University of Freiburg & Max-Planck Institute for Immunobiology, and CD23-cre mice[28] were obtained from Meinrad Busslinger at the Research Institute of Molecular Pathology, Vienna. All animals were maintained in the Laboratory Animal Center of the National Health Research Institute (NHRI). All experiments were approved by the Institutional Animal Care and Use Committee, NHRI. Mice of 8-12-week-old mice were used in experiments unless otherwise mentioned. Mice gender used in experiments was specified in figure legends.

## METHOD DETAILS

### B cell purification and cell culture

Freshly sorted FO and MZ B cells were preincubated with APC-conjugated anti-IgM (BioLegend) for 30 min on ice. After washing in ice-cold PBS, labeled cells were incubated at 37°C for 0, 15 or 60 min, respectively. The incubation was terminated by the addition of ice-cold RPMI 1640 (pH 2.5) to strip off surface-bound anti-IgM, followed by the fixation step using Cytofix Fixation Buffer (BD). The engulfed APC signals were determined by flow cytometry. % BCR endocytosis was calculated by [net stripped IgM$^+$ (at the time post stimulation, time x) - net stripped IgM$^+$ (at time zero)]/[net nonstripped IgM$^+$ (at time x) - net stripped IgM$^+$ (at time zero)] as previously reported.[50]

### B-cell purification, cell stimulation and drug treatment *in vitro*

Single-cell suspensions were prepared from mouse spleen by sieving and gentle pipetting through 70-μm nylon mesh filters (BD Falcon). Non-B cells were depleted by incubation with a cocktail of biotin-conjugated antibodies recognizing NK-1.1, Thy1.2 (CD90.2), Gr-1 (Ly-6G and Ly-6C), CD49b (DX5), CD11b, CD11c, and Ter-119 (BD), followed by enrichment by mixing with IMag Streptavidin Particles Plus beads (BD). Splenic B cells of purity between 94 and 98% were used in all experiments. For isolation of FO and MZ B cells, purified splenic B cells were suspended in FACS buffer [2%BSA/PBS, 2mM EDTA (pH 8.0), 0.1% $NaN_3$] and sorted by BD Influx with a 100-μm nozzle at 4°C. B cells were routinely cultured in 10%FBS/RPMI 1640 complete medium [supplemented with 2 mM L-glutamine (Gibco), 100 U penicillin-streptomycin (Gibco), 10 mM HEPES (Gibco), 0.055 mM 2-mercaptoethanol (Gibco), and 10% FBS (HyClone)]. B cells were stimulated with 1 μM CpG ODN1668 (denoted as CpG, InvivoGen), 10 ng mL$^{-1}$ CL307 (InvivoGen), 10 μg mL$^{-1}$ LPS (InvivoGen), or 5 μg mL$^{-1}$ poly(I:C) (InvivoGen) for 24 h. The sorted B cells were cultured in 10%FBS/RPMI complete medium for all experiments. To examine drug effects on IL-6 production, cells were stimulated 1 μM CpG combined with inhibitors including 10 mM NF-κB p65 inhibitor CAPE (Tocris), 5 mM NF-κB p50 inhibitor Kamebakaurin (MedChemExpress), 10 μM PIK3C3 inhibitor SAR405 (MedChemExpress), 20 nM INPP4 inhibitor bpV(phen) (Cayman), 100 μM Caveolin 1 inhibitor Methyl-β-cyclodextrin (MedChemExpress), 100 μM clathrin inhibitor MK-2206 dihydrochloride (MedChemExpress), 10 μM or 20 μM MyD88 inhibitor TJ-M2010-5 (MedChemExpress) for 24 h. Cells or the culture medium were collected and subjected to immunofluorescence experiments or ELISAs.

### ELISA

Serum IgM and IgG1 were captured by goat anti-mouse IgM (Southern Biotech) and IgG1 (Southern Biotech) antibodies which were coated on the surface of SpectraPlate-384 HB (PerkinElmer), and then those titers were detected by HRP-conjugated goat anti-mouse IgG (Jackson ImmunoResearch). Serum autoantibodies were determined by using an anti-dsDNA ELISA Kit (Fujifilm-Wako-Shibayagi) and an anti-nuclear antibody ELISA kit (antibodies-online). Serum IL-6 and TNF-α were detected by using the DuoSet ELISA kit (R&D Systems).

### Flow cytometry

Single cells (1x10$^6$) were washed twice with FACS buffer and maintained in the dark at 4°C throughout the experiments. A flow cytometer (CantoII; BD) and FACSDiva software (BD) were used to acquire flow cytometric data, and FlowJo software was used for analysis. For FACS staining, cells were incubated with anti-mouse antibodies on ice for 15 min to detect surface markers, or with antibodies for 45 min to detect intracellular molecules followed by two washes in FACS buffer. Viable cells were gated after staining with 7AAD (Sigma-Aldrich) or Fixable Viability Stain 620 (BD Horizon). For intracellular staining of cytokines, transcription factors or phosphoproteins, cells were fixed and permeabilized using the Transcription Factor Buffer Set (BD Pharmingen) prior to incubation with antibodies and according to the manufacturer's instructions.

### Immunofluorescence staining and Duolink proximity ligation assay (PLA)

Single splenic B cells were fixed and permeabilized using the Transcription Factor Buffer Set (BD Pharmingen) prior to blocking in Imag-iT FX Signal Enhancer (Invitrogen). Cells were then incubated with anti-TLR9 (Invitrogen) or anti-p-p38 Y182 (Cell Signaling) at 4°C overnight, followed by anti-rabbit IgG-Alexa488 (Invitrogen) as the secondary antibody for 1 h, or incubated with anti-BANK1 (Santa Cruz Biotechnology), anti-PI(3)P (Echelon Biosciences), and anti-LAMP1 (Cell Signaling), which were conjugated with fluorophore using the APEX Alexa Fluor 555 Antibody Labeling Kit (Invitrogen) at 4°C overnight. To stain LDs, cells were incubated with BODIPY 493/503 (Invitrogen) for 1 h. The PLA experiments were performed according to the manufacturer's procedure. Cells were fixed, permeabilized and incubated with anti-TLR9 and anti-PI(3)P antibodies as described above at 4°C overnight. Duolink *In Situ* PLA Probe Anti-Rabbit PLUS (Sigma-Aldrich) and Duolink *In Situ* PLA Probe Anti-Mouse MINUS (Sigma-Aldrich) were used to detect the primary antibodies. Duolink *In Situ* Detection Reagent Green (Sigma-Aldrich) was used for ligation and signal amplification. All cells were stained with DAPI (Invitrogen), air-dried on slides, and mounted using ProLong Gold Anti-fade Reagent (Invitrogen). Images were recorded using a Leica TCS SP5 II instrument (Leica Microsystems). Mander's coefficient was used as a parameter of colocalization and was calculated by Just Another Colocalization Plugin from ImageJ software.[51]

### Immunoblot assay and immunoprecipitation (IP)

For total lysate preparation, $1x10^7$ cells were lysed with 100 μL of 1% DDM lysis buffer [137.5 mM NaCl, 50 mM Tris (pH 7.8), 0.75 mM EDTA (pH 8.0), 1 mM sodium orthovanadate, 10% glycerol, 1% n-dodecyl β–D-maltoside (DDM), and freshly added protease inhibitors]. The lysates were then fractionated by SDS-PAGE and blotted using standard procedures. Proteins were detected using anti-BANK1 (Santa Cruz), p-p38 T180/Y182 (Cell Signaling), p38 (Cell Signaling), TLR9 (Invitrogen), Syk (Santa Cruz), NF-κB p105/p50 (Cell Signaling), and anti-β-actin (Cell Signaling) antibodies. For the IP experiment, anti-TLR9 (Invitrogen) and isotype control (Cell Signaling) were utilized. Blots were developed using Immobilon Western Chemiluminescent HRP Substrate (Millipore).

### Single-cell RNA-sequencing (scRNA-seq) and data analysis

Purified B cells were left unstimulated or stimulated for 2 h at 37°C with 1 μM CpG 1668, or 1 μM CpG plus 5 μM p38 inhibitor SB203580 (InvivoGen). Viable single cells were harvested for single-cell analysis using the BD Rhapsody system (BD) and transferred into nano-well cartridges loaded with Cell Capture Beads (BD Rhapsody) following the manufacturer's protocol. The single-cell RNA library was then established according to the manufacturer's instructions. The library containing 7754.72 molecule counts per gene per cell were recorded as a Fastqs file and uploaded to the Seven Bridges platform for data demultiplexed analysis (https://www.sevenbridges.com). Raw reads and processed data have been deposited at NIH GEO database under the access number GSE179715. After removing undetermined ($n$ = 317) and multiplet ($n$ = 2,137) cells, a total of 17,546 cells comprising 20,894 genes were subjected to *DotPlot*, *fgsea*, and *Heatmap* analyses implemented in *Seurat* (v4.1.0).[49]

### Quantification and statistical analysis

The results were represented as the mean ± SEM. Each representative data point was shown from at least two independent repeats. Statistical analysis was conducted by using GraphPad Prism v7.0 (GraphPad Software). Statistical differences were determined by an unpaired two-tailed t test with $p$ values $\leq 0.05$.